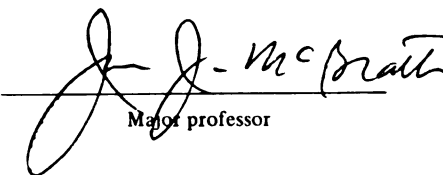




LIBRARY
Michigan State
University

This is to certify that the
thesis entitled
**Experimental Measurement of the
Slit Response Function and
Corrected Infrared
Thermographic Measurements**
presented by
Paul Bryan Hoke

has been accepted towards fulfillment
of the requirements for
MS degree in Mechanical Engineering


Major professor

Date August 21, 1998

PLACE IN RETURN BOX to remove this checkout from your record.
 TO AVOID FINES return on or before date due.
 MAY BE RECALLED with earlier due date if requested.

DATE DUE	DATE DUE	DATE DUE
MAY 05 2003		
OCT 26 2003		
APR 17 2004		
OCT 30 2003		

**EXPERIMENTAL MEASUREMENT OF THE SLIT RESPONSE FUNCTION AND
CORRECTED INFRARED THERMOGRAPHIC MEASUREMENTS**

By

Paul Bryan Hoke

A THESIS

**Submitted to
Michigan State University
in partial fulfillment of the requirements
for the degree of**

MASTER OF SCIENCE

Department of Mechanical Engineering

1998

ABSTRACT

EXPERIMENTAL MEASUREMENT OF THE SLIT RESPONSE FUNCTION AND CORRECTED INFRARED THERMOGRAPHIC MEASUREMENTS

By

Paul Bryan Hoke

Infrared thermography utilizes emitted radiation to measure temperatures optically. An experimental facility and procedures were defined to measure emissivity and temperature of unresolved (target angle < 0.05 rad) targets. The facility consists of a flow system with instrumentation for measuring flow velocity, temperature, and humidity. The emissivity is determined with the infrared camera and the target temperature set by the known flow conditions. Once the specimen emissivity and size are known, its temperature can be measured in any environment.

An Inframetrics 600L infrared camera and the associated data acquisition system were characterized to maximize thermal measurement sensitivity. The minimum specimen size that can be resolved thermally with the infrared camera was determined. The effect of specimen size on thermal signature was quantified for the infrared detector utilizing the slit response function (SRF). A standard procedure to measure emissivity was validated and a SRF measurement correction was verified. These two pieces of information increased the measurement capabilities of the infrared system and minimized experimental error when working with thermal targets smaller than the thermal measurement resolution of the system.

To Carol,
for always believing
and of course, Madeleine

ACKNOWLEDGMENTS

I would like to thank my advisor Dr. John McGrath for having the patience to let me try things on my own and guiding me when I needed it. His advice, insight and assistance to this work have been invaluable.

I would also like to thank Dr. Craig Somerton and Dr. Andre Benard for joining my committee and editing this work.. Dr. Somerton has been an aid through out my stay at Michigan State University as an advisor, reference and an open door. Dr. Benard's aid and insight are greatly appreciated.

Dr. Foss for his advice, guidance, and equipment. Dr. Foss was a wealth of support and knowledge, especially on the finer points of fluid mechanics.

Mike McClean for his mechanical assistance and precision work.

The aide I have received from my colleagues has been immeasurable. Heidi Relyea, Jon Darrow, Al Aksan, Ramez AbdulNour, Mark Minor, Gloria Elliot, Bin Lian, Ingo John, Doug Neal and Scott Morris have all helped me out along the way. It ranged from moving equipment, helping solve nasty mathematical problems, studying for class, or just listening, but it all helped me through and for that I say thanks!

TABLE OF CONTENTS

LIST OF TABLES	vii
LIST OF FIGURES	viii
NOMENCLATURE	xi
CHAPTER 1. INTRODUCTION	1
CHAPTER 2. WIND TUNNEL TEST FACILITY	4
2.1 DESIGN OBJECTIVES	4
2.2 WIND TUNNEL BASE	6
2.3 TEST MODULE	7
2.4 THROTTLE ASSEMBLY	9
2.5 FLOW CONDITIONING	10
2.6 DATA ACQUISITION	12
2.7 PRESSURE MEASUREMENT	13
2.8 HOT WIRE SENSORS	13
2.9 CALIBRATION NOZZLE AIRFLOW HEATER	14
2.10 CHARACTERIZATION OF THE WIND TUNNEL FACILITY	15
2.11 SUMMERY	19
CHAPTER 3. CALIBRATION OF INFRAMETRICS IR CAMERA AND ASSOCIATED DATA ACQUISITION SYSTEM.....	20
3.1 INTRODUCTION.....	20
3.2 STATEMENT OF PROBLEM	20
3.3 EXPERIMENTAL PROCEDURE	22
3.4 RESULTS	27
3.5 OPTIMAL CONFIGURATION TESTING	31
3.6 RESULTS OF OPTIMIZED EQUIPMENT CONFIGURATION	31
CHAPTER 4. SLIT RESPONSE FUNCTION	34
4.1 INTRODUCTION	34
4.2 IMAGE PROCESSING EFFECTS ON DATA	38
4.3 EXPERIMENTAL TEST PROCEDURE	39
4.4 RESULTS	41
4.5 PREDICTIVE CAPABILITIES	44
4.6 CONCLUSIONS	47

CHAPTER 5. EXPERIMENTAL VERIFICATION OF THERMOGRAPHIC TEMPERATURE MEASUREMENT UTILIZING SLIT RESPONSE CORRECTION.....	49
5.1 INTRODUCTION	49
5.2 EXPERIMENTAL PROCEDURE	49
5.3 EMISSIVITY MEASUREMENT	51
5.4 EXPERIMENTAL VERIFICATION	53
5.5 DISCUSSION	63
CHAPTER 6. CONCLUSIONS	69
CHAPTER 7. RECOMMENDATIONS FOR FUTURE WORK.....	73
7.1 SLIT RESPONSE FUNCTION	73
7.2 INFRARED CAMERA RESPONSE TO TEMPERATURE GRADIENTS.	73
7.3 HOT-WIRE SENSORS	74
7.4 DATA ACQUISITION SYSTEM	75
APPENDICES	79
APPENDIX 1. TWO DIMENSIONAL FLOW CONTRACTION	80
APPENDIX 2. QUICKBASIC[®] PROGRAM TO PERFORM DATA ACQUISITION AND STEPPER MOTOR CONTROL	84
APPENDIX 3. FLAT PLATE ISOTHERMAL VELOCITY PROFILES	108
APPENDIX 4. HOT-WIRE CONSTRUCTION AND CALIBRATION	111
APPENDIX 5. MAXIMIZING THE DYNAMIC RESPONSE OF THE INFRAMETRIX IR CAMERA AND DATA RECORDING SYSTEM	121
APPENDIX 6. VELOCITY AND TEMPERATURE CALCULATION PROGRAM FOR TWO HOT-WIRE METHOD	124
BIBLIOGRAPHY	129

LIST OF TABLES

Table 1. SRF summary for the Inframetrics 600L infrared camera in the HTRL	48
Table 2. Emissivity measurement results ($\epsilon=0.88$)	54
Table 3. Test results from test 1a (MAF sensor) (11 amps to flow heater, 42.1-62.1 ⁰ C IR temperature range) ...	56
Table 4. Test results from test 1b (MAF sensor) (4 amps to flow heater, 20.0-40.0 ⁰ C IR temperature range)	57
Table 5. Emissivity measurement results ($\epsilon=0.95$)	59
Table 6. Test results from test 2a (11 amps to flow heater, 32.9-52.9 ⁰ C IR temperature range) ...	61
Table 7. Test results from test 2b (6 amps to flow heater, 23.3-43.3 ⁰ C IR temperature range) ...	62
Table 8. Null hypothesis statistical test results	68
Table 9. Two dimensional contraction machining coordinates	81
Table 10. Post calibration data	119

LIST OF FIGURES

Figure 1. Wind tunnel test facility concept drawing	4
Figure 2. Wind tunnel test facility	5
Figure 3. Modular concept utilized to guide flow facility design	6
Figure 4. Structural drawing of sub-atmospheric test section	8
Figure 5. Sluice throttle mechanism used to control airflow rates (top view)	10
Figure 6. Airflow conditioner	11
Figure 7. Calibration nozzle airflow joule heater	15
Figure 8. Axi-symmetric calibration nozzle and associated coordinate system	17
Figure 9. Calibration nozzle exit velocity profile	17
Figure 10. Calibration nozzle exit temperature profile	18
Figure 11. Ideal gray scale-temperature response for the Inframetrics infrared camera and associated data acquisition system	21
Figure 12. IR camera tool for area temperature measurement	22
Figure 13. Schematic of different equipment configurations tested	23
Figure 14. Playback data image sequence from the equipment test experiment conducted on 2/11/97.....	25
Figure 15. Equipment configuration effects on the IR camera gray scale-temperature response	28
Figure 16. Comparison of equipment tests with and without the For-A VTG-33 video timer	29
Figure 17. IR camera gray scale output as a function of contrast setting. (Low end of Inframetrics camera temperature scale)	30

Figure 18. Gray scale-temperature relationship with optimal contrast settings	32
Figure 19. Optimal equipment configuration gray scale-temperature relationship	33
Figure 20. Schematic of IR camera optical configuration and definition of terms.....	35
Figure 21. Comparison of scan direction effect on IR camera response	36
Figure 22. Temperature profile of narrow dimension of the MAF sensor. Sensor parallel to scan direction	37
Figure 23. Temperature profile of narrow dimension of the MAF sensor. Sensor perpendicular to scan direction	37
Figure 24. Schematic of the experimental configuration for SRF measurement	39
Figure 25. Slit response function with 95% confidence region (n=5) for the Inframetrics 600L IR camera	41
Figure 26. SRF confidence region/mean value for Inframetrics 600L IR camera with external optics	42
Figure 27. SRF of the Inframetrics 600L infrared camera with 3x Telescopic and 6" close lenses	43
Figure 28. Thermographic image of MAF sensor	44
Figure 29. Comparison of SRF between system configurations (no optics compared to external optics).....	47
Figure 30. Emissivity variation observed in semi-conducting materials by Inagaki et.al., 1994	65
Figure 31. Correction factor (1/SRF) and % uncertainty in CF for Inframetrics 600L IR camera with close up optics in place as a function of target size	71
Figure 32. Cumulative average of the hot-wire data	77
Figure 33. Two-dimensional flow contraction	80

Figure 34. Compiled jet velocity profiles ($w=2\text{cm}$)	109
Figure 35. $X/W=1.59$ velocity profiles ($w=2\text{cm}$)	109
Figure 36. $X/W=4.52$ velocity profiles ($w=2\text{cm}$)	110
Figure 37. $X/W=10.95$ velocity profiles ($w=2\text{cm}$)	110
Figure 38. Schematic of hot-wire probe	111
Figure 39. Tungsten wire copper plating station	112
Figure 40. Precision solder station	113
Figure 41. TSFL hot-wire calibration flow contraction	114
Figure 42. “Coke Bottle” contraction utilized for hot-wire calibration	115
Figure 43. TSFL contraction hot-wire calibration curve	117
Figure 44. HTRL facility hot-wire calibration curve	118
Figure 45. Optimal equipment configurations for data acquisition and processing	122
Figure 46. Results of optimized equipment configuration	123

NOMENCLATURE

ENGLISH:

A	Area
A,B,n	Hot-wire calibration coefficients from Collis and Williams [1959]
ATF	Aperiodic transfer function
C _d	Discharge coefficient
D	Diameter
E	Voltage
E _b	Blackbody emissive power (W/m ²)
h	Convective heat transfer coefficient
IR	Infrared
J	Radiosity
L	Confidence region
MAF	Mass air flow
P	Pressure
Pr	Prandtl number
Q	Thermal energy
Q _R	Radiated flux
R(λ)	Wavelength dependent radiosity
Re	Reynolds Number (=Ux/ ν)
SRF	Slit response function
T	Temperature

T^*	Non-dimensionalized temperature $[(T - T_{\text{range-Min}})/T_{\text{range}}]$
T_{actual}	True temperature value
T_{IR}	Infrared measured temperature
T_{MAF}	MAF sensor temperature
T_{range}	Temperature span on infrared camera
$T_{\text{range-Min}}$	Lower limit of temperature span on infrared camera
T_{SRF}	Infrared measured, SRF corrected temperature
U	Streamwise velocity
V	Velocity
V_{max}	Maximum velocity
W	Wall jet slot width
f	Focal distance
g	Acceleration due to gravity
k	Thermal conductivity
l_d	Working distance
l_s	Slit width
l_i	Internal focal length
n	Number of data points
t	Statistical parameter from student T distribution
x	Streamwise direction
y	Direction orthogonal to streamlines and test plate
z	Direction aligned with gravity or direction orthogonal to xy plane - context will clarify

GREEK:

Φ	Measurement error
Θ	Target angle
Ω	Electrical resistance
α	Absorbitivity
ϵ	Emissivity
λ	Wavelength
ρ	Density or Reflectance - Context will clarify
σ	Standard deviation or Stephan-Boltzmann constant - context will clarify
τ	Transmissivity
ν	Kinematic viscosity

CHAPTER 1. INTRODUCTION

1.1 MOTIVATION

The original motivation for this study was provided by a project for General Motors Corporation. The manufacturing process of mass air flow (MAF) sensors for an engine intake manifold requires that each sensor be individually calibrated. The calibration method utilized was expensive and time consuming. The method consisted of mounting the MAF sensor in a mold and filling the mold with an isothermal, electrically neutral and environmentally friendly liquid. This created an environment of known temperature in which the sensor resistance could be measured. The method provided a two point temperature-resistance calibration curve. The material cost for the fluid utilized was approximately 1.5 million dollars per year not incorporating the energy costs of heating it. Infrared thermography and an alternate heating method were proposed to obtain the necessary temperature/resistance information in order to replace the current calibration method.

The project was complicated by the size and material characteristics of the MAF sensor. The sensor is a 1500 μm long and 500 μm diameter cylinder constructed from platinum wire surrounded by a glass body. The glass surface could not be coated with any materials and was expected to experience a large amount of manufacturing variability. Thus, the problem of measuring the surface temperature the small sensor size was complicated by unknown and variable emissivity properties of the specimen.

A wind tunnel facility was constructed to support and augment the Heat Transfer Research Laboratory (HTRL) and specifically to investigate the capabilities of the infrared measurement equipment. This facility was designed to provide a flow of known velocity

and temperature and the sensors necessary to monitor this flow. Chapter 2 details the wind tunnel facility and its construction, the data acquisition system, and the measurement transducers utilized. This facility development was essential as a test platform for the current project.

The laboratory utilizes an Inframetrics 600L infrared camera and the associated data acquisition system to obtain spatial temperature information. This system was characterized and optimized to obtain the full dynamic temperature measurement range. The effects of specimen size on the measurement capabilities were determined experimentally utilizing the slit response function (SRF) of the infrared sensor. The SRF is the attenuated response of the sensor to targets smaller than its measurement resolution.

The combination of the flow facility and the characterization of the infrared system allow the goals of the original proposal to General Motors to be realized.

1.2 PREVIOUS WORK

The capabilities and applications of infrared thermographic equipment have been explored by a previous investigators. The sensors response to an unresolved target (subtends an angle less than the measurement capabilities of the sensor) has been explored extensively by Holst [1993]. The target angle to produce a 50% response (the 50% slit response function (SRF)) is generally provided by the manufacturer of the equipment as a measure of the performance (Inframetrics [1988]). These quantities are provided to define the limitations of the equipment so as to avoid inaccurate measurements. It is the goal of this study to quantify the slit response function to allow meaningful measurements to be

taken in these circumstances and thus to exploit the maximum capabilities of the infrared camera systems.

Infrared thermography has also been applied in wind tunnel studies of fluid mechanics and heat transfer. One application has been the study of supersonic heating of structures (Lafferty and Collier [1991]). Infrared thermography has also been applied to study the surface temperature of structures in flows to measure the convective heat transfer coefficient (Willenborg, et al. [1996], Okamoto and Inagaki [1994]).

Gartenburg and Roberts [1990] studied the temperature gradients on a heated wire in a flow field with an infrared imaging system. The study involved imaging an unresolved target (the wire) and compensating for the error in the temperature by using an 'apparent' emissivity. This method compensated for the targets emittance and size but the study was fixed in one configuration because a change in the working distance caused a change in the apparent emittance.

This study involved calibrating an infrared camera and the associated data acquisition system. An ideal linear system response to temperature was defined to maximize the dynamic range and the equipment was configured to obtain this result. The infrared camera response to unresolved targets was determined experimentally. A wind tunnel facility with well characterized flow conditions was developed to support the experimental work and a series of experiments to validate and explore the infrared data acquisition system were conducted.

CHAPTER 2. WIND TUNNEL TEST FACILITY

2.1 DESIGN OBJECTIVES

A wind tunnel testing facility was built to advance the laboratory testing capabilities and to generate constant temperature and velocity flow conditions. The facility was designed to allow calibration of various sensors, to achieve specific testing goals as well as to allow for future expansion. The entire system was designed to be modular so that any component could be replaced with minimal effort (Figure 1).

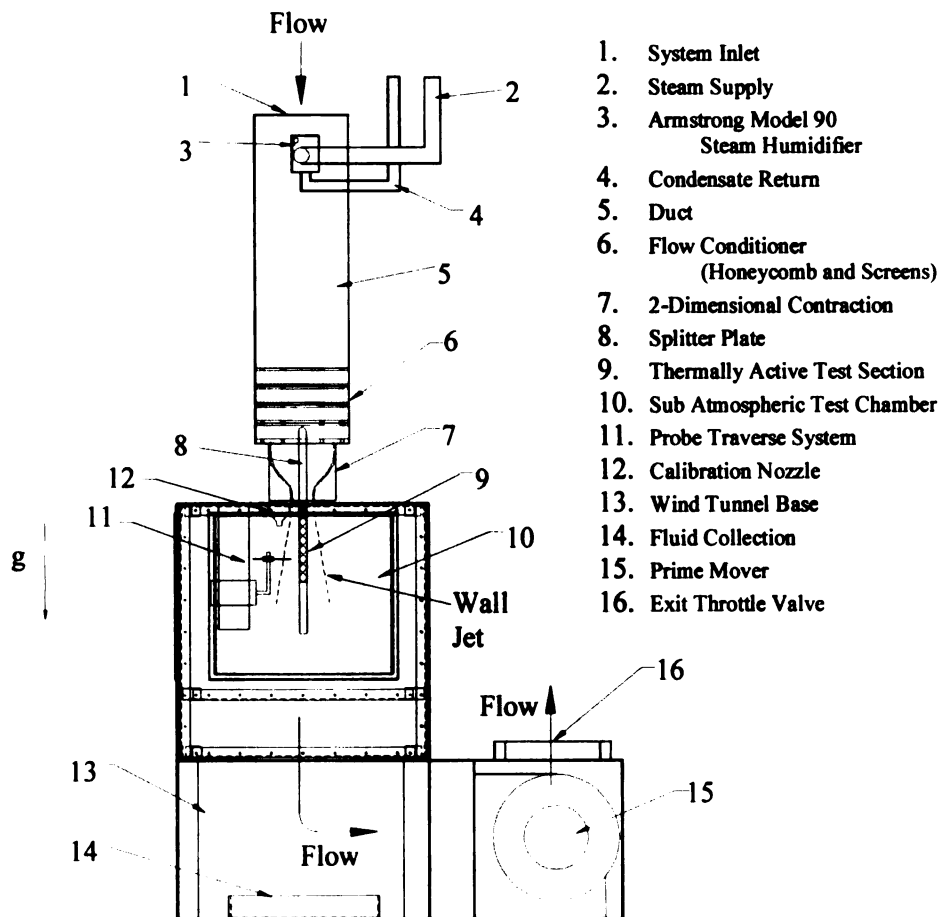


Figure 1. Wind tunnel test facility concept drawing.

Several physical quantities are controlled or measured in this facility so that the target emissivity and temperature can be obtained with infrared thermographic techniques. These include: pressure (and thus mean flow velocities), velocity and temperature of the air flow. Humidity of the air flow was measured but not controlled in this study. Specific controls or measurement sensors are described and their application to the infrared testing procedure are defined in this chapter.

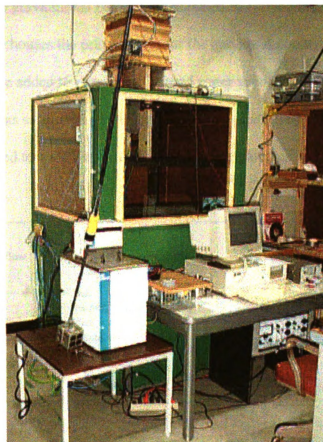


Figure 2. Wind tunnel test facility.

2.2 WIND TUNNEL BASE

The base of the testing apparatus was designed to fulfill several functions. The base design followed the modularity concept for the entire system. This concept allowed different flow configurations with respect to the test piece and the gravitational field to maximize testing flexibility. The design allows for the air flow to be oriented in the same or opposite direction as the gravitational field (Figure 3). Air flow orthogonal to gravitational field can be obtained by turning the system on its side. The base structure houses the prime mover for the system. A condenser and drain section may also be added to remove condensed water vapor for future experiments. The test section was supported physically by the wind tunnel base section. The entire structure was sealed to maintain a vacuum during operation.

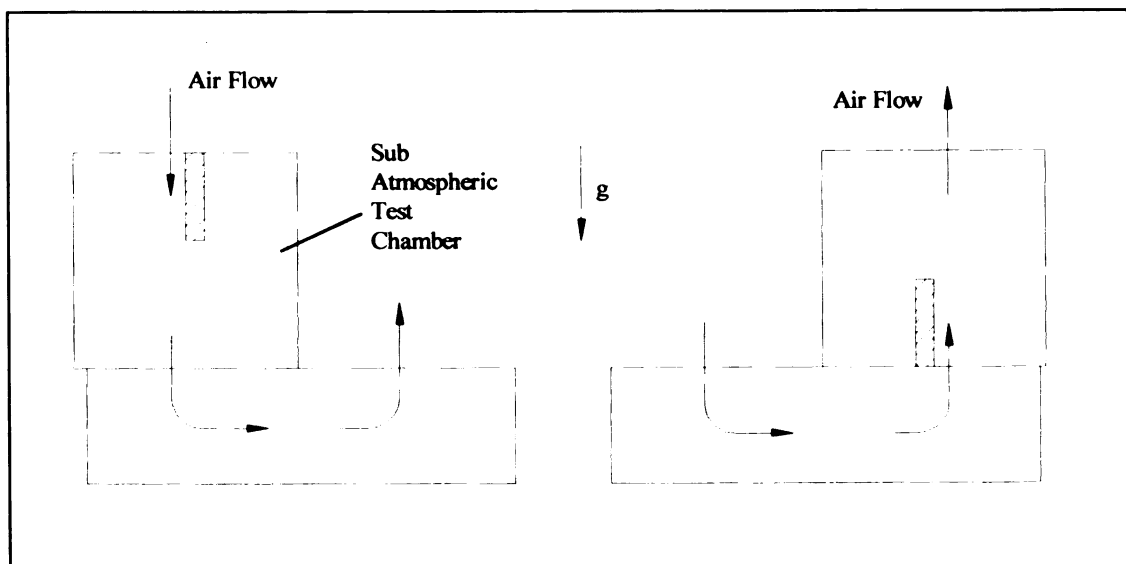


Figure 3. Modular concept utilized to guide flow facility design.

The base was constructed with 2"x4" boards for the support structure and covered with sheets of 15/32" plywood. These materials were chosen to reduce costs and allow for easy and inexpensive modifications. The assembly was completed with 3/8" hex head bolts and wood screws to allow for easy disassembly if necessary.

The joints were sealed with GE silicon sealant. One end of the base structure was designated as a door and made removable to allow access to the interior. The access regions were taped with closed cell foam tape to seal the unit while it was operational. The interior wood surfaces were treated with a wood preservative to protect against water damage resulting from high humidity experiments.

2.3 TEST MODULE

One of the primary design requirements for the test section was to allow variable orientation of the test section with respect to gravity. The test section was thus designed as a cube so that the sides could be interchanged to accommodate different testing configurations. The simplicity of this design (Figure 4) was its greatest strength. Two sides of the module have 0.375" thick plate glass to allow optical access to the interior environment. One side was designed with a removable door and the remaining side was solid. The top and bottom of the module have openings appropriate to the air passage through the respective sides.

The frame of the test section was constructed of 2"x2" angle iron with a 15/32" skin of plywood. The plywood skin was bolted onto the iron frame for easy modifications and reconstruction. The interior of the testing module was treated with shellac to prevent degradation of the wood during experiments with high humidity.

Four extra 2"x2" angle iron support members were included in the original design.

These members (Figure 4) can be utilized for additional support if necessary or to mount equipment in the testing environment.

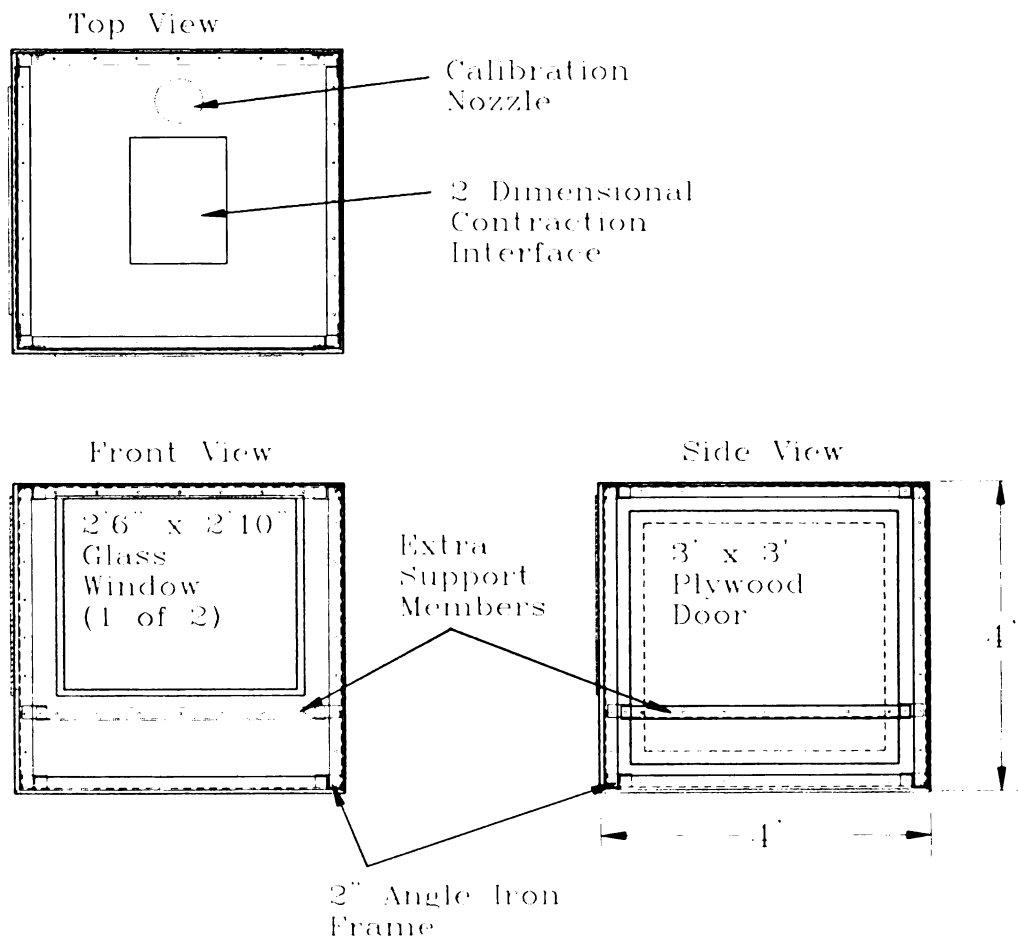


Figure 4. Structural drawing of sub-atmospheric test section.

2.4 THROTTLE ASSEMBLY

Fine control of air flow rate through the system was required to allow hot wire calibration and to insure experimental reproducibility. A “sluice” style throttle valve at the exit of the facility was chosen for its simplicity and its proven effectiveness in the Turbulent Shear Flows Laboratory (TSFL) at Michigan State University.

To form the sluice, a plywood gate was mounted between two 2”x 4” boards with bearings to allow smooth movement. Two 1”x 1” angle irons lined with Teflon strips were mounted above the plywood gate to seal the edges. Teflon was chosen because of its low friction characteristics which prevented the throttle from binding. The final throttle assembly is shown in Figure 5. The throttle system was sensitive enough to allow hot wire calibration and to maintain steady flow conditions during velocity profile measurements. The pressure drop between the sub-atmospheric test chamber can be controlled from 0.010 to 0.50 inches of H₂O which results in a velocity range of 2.03 to 14.40 m/s through the calibration nozzle. (The velocity was calculated utilizing the Bernoulli equation rearranged as

$$V_2^2 - V_1^2 = \frac{2(P_1 - P_2)}{\rho} - g(z_1 - z_2). \quad (1)$$

Assume $V_1 \approx 0$, and $-g(z_1 - z_2) \approx 0$ results in:

$$V_2 = \sqrt{\frac{2(P_1 - P_2)}{\rho}} \quad (2)$$

These equations assume incompressible, inviscid, steady flow along a stream line through the nozzle). The pressure can be controlled by sluice position to increments of approximately 0.001 in-H₂O which was within the resolution limits (0.0025 inH₂O) of

the pressure transducer. This corresponds to a velocity resolution of approximately ± 5 cm/s at typical experimental flow settings.

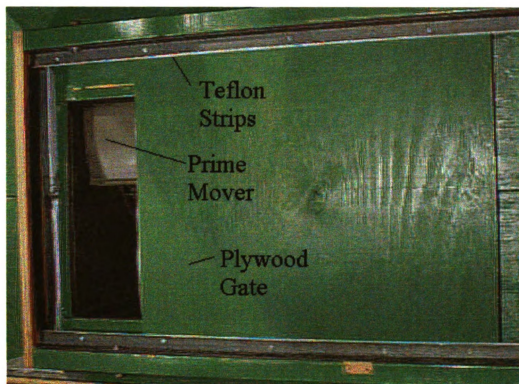


Figure 5. Sluice throttle mechanism used to control airflow rates (top view).

2.5 FLOW CONDITIONING

A structure was built for flow conditioning at the inlet of the system. This structure was designed to remove variability caused by changing ambient conditions and was necessary to insure experimental reproducibility and flow homogeneity. This system consists of a preconditioner and a flow contraction (Figure 6). The pre-

conditioner consists of 3 wire screen stretchers and a honeycomb straw structure. The contraction is two-dimensional and constructed from $\frac{1}{4}$ " thick Lexan[®].

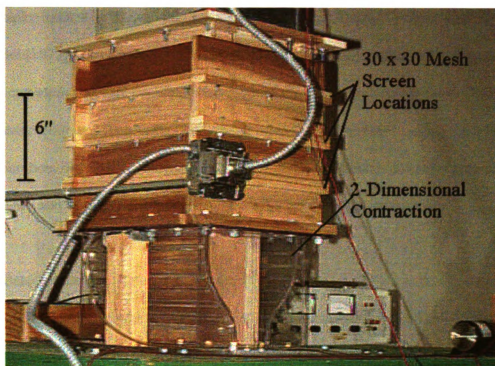


Figure 6. Airflow conditioner.

The design of the preconditioner was based on a design from the TSFL and the assistance of Professor Foss. The honeycomb structure removes large scale turbulent momentum eddies from the fluid. The wire screen used consisted of 30 x 30 wires per square inch mesh. This mesh removes smaller scale eddies from the fluid. The wire meshes were placed 3.5" apart. The disturbances created by the previous mesh are greatly dampened prior to reaching the next mesh (Blevins [1984]) at this distance.

A two dimensional contraction was utilized to accelerate the flow and to provide a uniform velocity profile at the contraction exit plane. The wall curvature was the critical design criteria for the flow contraction. The design was obtained from the principles defined in “Design of Two-Dimensional Wind Tunnel Contractions” by Morrel [1977]. The mechanical details of the contraction are presented in Appendix 1. This curvature prevents thick boundary layers from being produced at the exit plane of the contraction and it prevents flow separation in the contraction resulting from flow acceleration. The design accomplishes these ends by maintaining favorable pressure gradients and smooth transitions throughout the length of the contraction.

2.6 Data Acquisition System and Motion Control

A Keithley MetraByte DAS-TC data acquisition board and a DAS-02 analog output board were utilized with software written in QuickBasic[®] (Microsoft [1988]) (the QuickBasic program is presented in Appendix 2). These two boards can sample 16 channels of data and are capable of 2 channels of analog output. The DAS-TC board was utilized to obtain temperature and voltage measurements and the DAS-02 to output voltage control signals to a VCO-4050 stepper motor controller. The voltage measurements were from the hot wire anemometer, the pressure transducer, the humidity probe and the stepper motor control signal.

The VCO-4050 stepper motor controller and a CMD-50 chopper driver from American Precision Inc. and the Eastern Air Devices Model #LA23ECK-81 step motor with the custom built traverse system allowed the hot wire sensors to be moved in increments of $6.6\ \mu\text{m}$.

2.7 Pressure Measurement

A MKS Baratron Type 225A pressure transducer with a $\frac{1}{2}$ " H₂O full scale reading was utilized to measure pressure differentials in the system. These pressure measurements were used to calculate velocities for hot wire calibrations and to meter the flow for the actual experimental work. The MKS transducer can resolve pressure measurements with an accuracy of ± 0.0025 " H₂O. The relationship between velocity and pressure in the calibration nozzle is defined in Equation 1. The transducer was utilized to read the pressure drop across the contraction as well as the pressure difference between the atmosphere and the interior of the test section. Measurement of the pressure drop through the contraction allows for the inviscid core velocity in the test section to be calculated. This velocity was utilized to non-dimensionalize the experimental results. The pressure difference between the atmosphere and the sub-atmospheric test section allows the inviscid velocity through the calibration nozzle to be calculated.

2.8 Hot Wire Sensors

The hot wire sensors utilized in this facility consist of 5 μm diameter tungsten wire controlled by a TSI constant temperature anemometer (CTA) system (model 1051-2). The wires are powered electrically to produce an elevated temperature to maintain the prescribed resistance value. The CTA system utilizes a bridge circuit to control the current through the hot wire sensor and thus its resistance. The CTA system outputs the voltage signal required to maintain the sensor resistance. This voltage signal can be correlated with a known flow rates (through the calibration

nozzle) to calibrate the hot wire sensor so that it can be used to measure unknown flow velocities. The calibration results from a balance between the electrical heating of the sensor and the convective heat transfer. The governing equation used during the calibration is

$$E^2 = A - BV^n. \quad (3)$$

Essentially, the square of the voltage output (E) from the anemometer bridge was related to the velocity (V) by three calibration coefficients (A, B, and n). The hot wires are capable of measuring velocities within the range of the calibration to a resolution of $\pm 2\%$.

2.9 CALIBRATION NOZZLE AIRFLOW HEATER

A stainless steel 30 x 30 wires per inch mesh screen was utilized to heat the flow through the calibration nozzle (Figure 7) to provide an thermal energy source to heat the thermographic targets. The mesh has a resistance of 2Ω and was heated electrically with a HP6274B DC power supply. The low resistance of the screen requires a power supply with a high amperage output to supply adequate energy to the flow. The power supply was capable of providing 15 amps (30 watts).

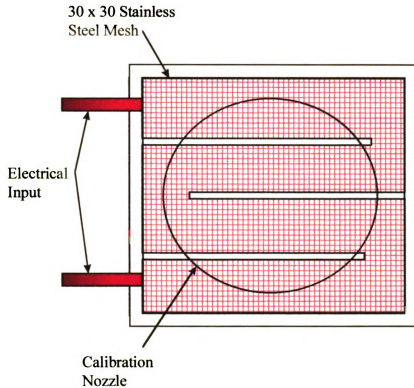


Figure 7. Calibration nozzle airflow joule heater.

The screen was able to create a temperature rise of 30°C above ambient when powered by 8 amps with an output flow velocity of 10 m/s through the calibration nozzle. The core of the flow has a measured temperature stability of $\pm 1.5^{\circ}\text{C}$. The design utilized presently was limited to 9 amps due to electrical arcing.

2.10 CHARACTERIZATION OF THE WIND TUNNEL FACILITY

Velocity profiles of the flows through the calibration nozzle and the two-dimensional contraction exit were obtained. Only the calibration nozzle was used in

the current study. However, the test section results were obtained to explore the capabilities of the facility and there are presented in Appendix 3 for completeness. Figure 8 shows the calibration nozzle schematically and the coordinate system used. Figure 9 shows the velocity profile at $X/D = 0.5$ in the calibration nozzle.

The majority of the exit area of the nozzle has a laminar uniform velocity profile. The flow was determined to be laminar from the hot wire voltage signal. This signal appeared smooth on an oscilloscope and had an RMS value of 2% of the mean flow value. It was important to note that the Reynold's number,

$$Re_D = \frac{U \cdot D}{\nu}, \quad (4)$$

based on the flow velocity and the nozzle exit diameter was equal to approximately 13,000. This number seems high enough to indicate that the flow should be turbulent, but because the flow was still developing, the central region of the nozzle was still unsheared and laminar.

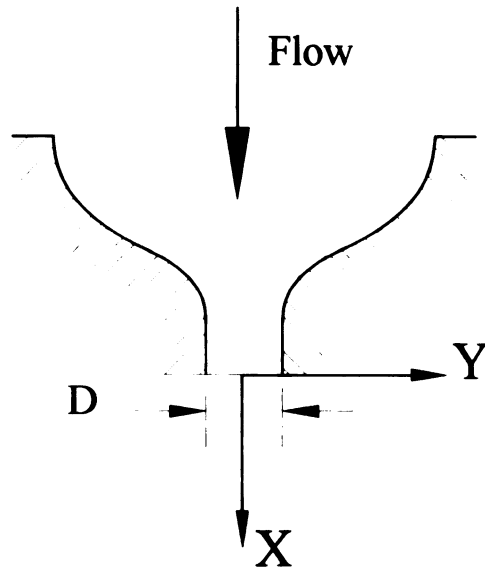


Figure 8. Axi-symmetric calibration nozzle and associated coordinate system.

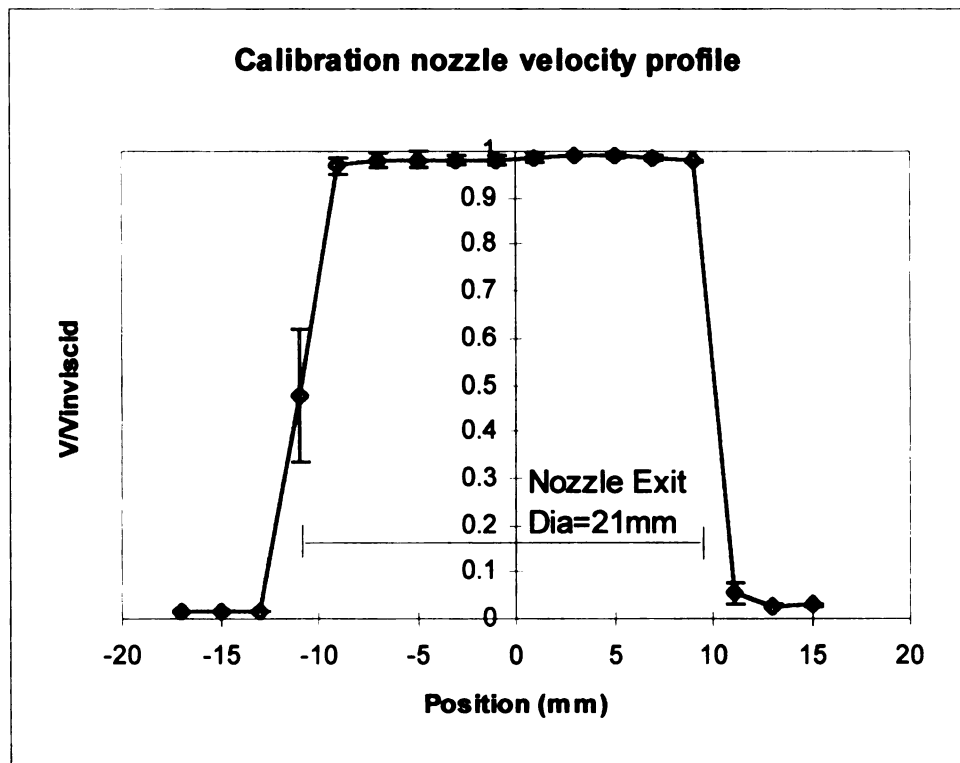


Figure 9. Calibration nozzle exit velocity profile.

Temperature profiles of the air at $X/D = 0.5$ below the exit plane of the calibration nozzle were also obtained. The profile for 10 m/s inviscid flow velocity and ambient temperature equal to 22°C with 8 amps and 6 amps provided to the flow heater are shown in Figure 10.

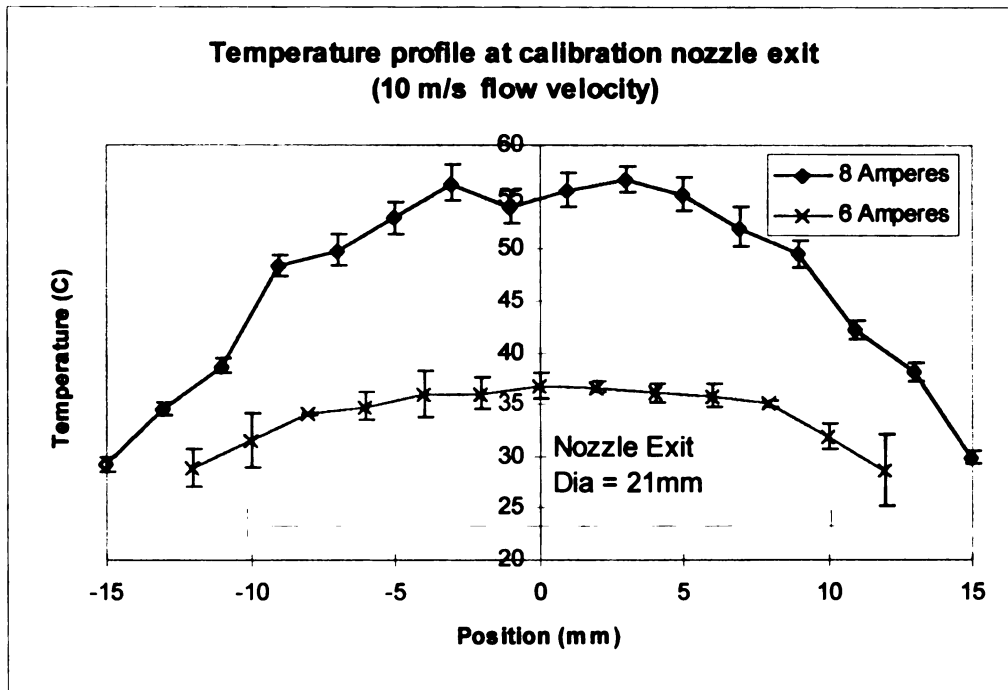


Figure 10. Calibration nozzle exit temperature profile.

This figure shows that there was a core of relatively constant temperature approximately 1 centimeter in diameter for each current setting. This was much larger than the specimens that were tested and was considered adequate for this study. The stability of $\pm 1.5^{\circ}\text{C}$ was larger than the uncertainty of the infrared camera ($\pm 0.3^{\circ}\text{C}$) utilized but appeared to be the stability limit of the heating system used. The room

temperature above the nozzle inlet was monitored and it experienced a standard deviation of approximately ± 1 °C over time period of 1 minute. This variation in the ambient conditions probably accounts for the majority of the fluctuation found in the nozzle temperatures.

2.11 SUMMARY

A wind tunnel facility was developed with the capability to create and monitor a flow with acceptably uniform velocity and temperature profiles in core regions of the calibration nozzle. The velocity, temperature and humidity of the flow can be individually measured and recorded with the data acquisition system. Fine motion control to position the sensors was obtained with stepper motors and a translation stage. This facility was characterized specifically to obtain measurements with infrared thermography of temperature and emissivity of optically unresolved specimens and to support other research projects in the Heat Transfer Research Laboratory (HTRL).

CHAPTER 3. CALIBRATION OF INFRAMETRICS IR CAMERA AND ASSOCIATED DATA ACQUISITION SYSTEM

3.1 INTRODUCTION

Infrared cameras produce temperature data as a function of spatial location and time. The appropriate data recording system typically includes a time marking video overlay, a video recording system (VCR), video monitors and image processing software to analyze the data. The video overlay allows time data to be saved simultaneously with the temperature field information. The video recording system allows data storage and post processing of the information. The experiments can be viewed in real time on the video monitors. The software allows digitizing of the video signal and provides necessary quantitative analysis tools.

The following equipment were available to achieve these functions: an Inframetrics 600L infrared camera; a For-A VTG-33 video timer; a Sony PVM-1343MD Trinitron monitor; a Panasonic AG-2400 monitor and Image Pro Plus v2.1 (Media Cybernetics [1995])..

The interfacing and optimization of this system to obtain optimal experimental analysis is explored in this chapter. An ideal system response is outlined and an equipment arrangement to achieve that response is defined.

3.2 STATEMENT OF PROBLEM

The Inframetrics infrared camera outputs an 8 bit digital signal in RS170 video format that includes the temperature field information. An ideal system output is defined

for this work as linear response that spans the entire dynamic range (Figure 11). The linearity of the output maintains uniform sensitivity over the experimental range and simplifies processing.

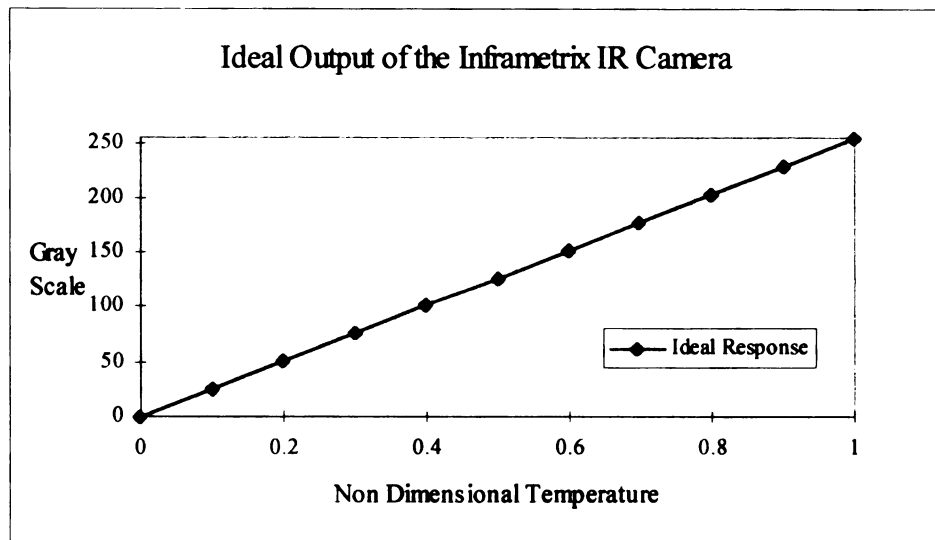


Figure 11. Ideal gray scale-temperature response for the Inframetrics infrared camera and associated data acquisition system.

Different equipment or equipment arrangements are often utilized in the data recording circuit depending on the experiment, experiment location (the camera is portable), and equipment available . There was evidence that different equipment combinations could result in variations in the data when data obtained at the top of the Inframetrics camera range would saturate at different levels for different users. It was determined that this was directly caused by the data recording and processing equipment.

3.3 EXPERIMENTAL PROCEDURE

3.3.1 EXPERIMENTAL CONFIGURATION

An HP-6236B Triple output power supply powered a plate heater to a temperature between 5 and 10 degrees centigrade above ambient temperature. The plate temperature was monitored with a calibrated T-type thermocouple ($\pm 0.1^{\circ}\text{C}$ accuracy). The IR camera was then set with its temperature range lower limit just below the plate temperature. The system was allowed to stabilize for 15 minutes to insure it was at steady state. The IR camera was then used to define the plate temperature field with several different equipment arrangements. The area function of the IR camera was used to define the region of interest (Figure 12). This insured that the same surface area was analyzed each time. This avoided variability due to non-uniform surface properties on the plate.

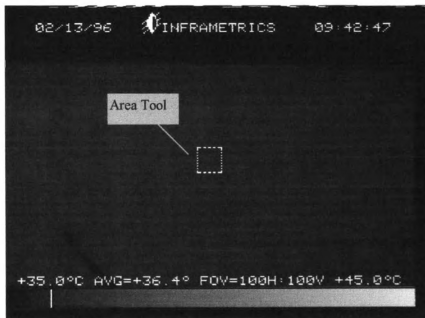


Figure 12. IR camera tool for area temperature measurement.

Data were obtained with a variety of equipment configurations. These equipment arrangements were chosen to represent potential data acquisition arrangements or systems that are currently being utilized in the laboratory. The different equipment configurations that were tested are shown schematically in Figure 13.

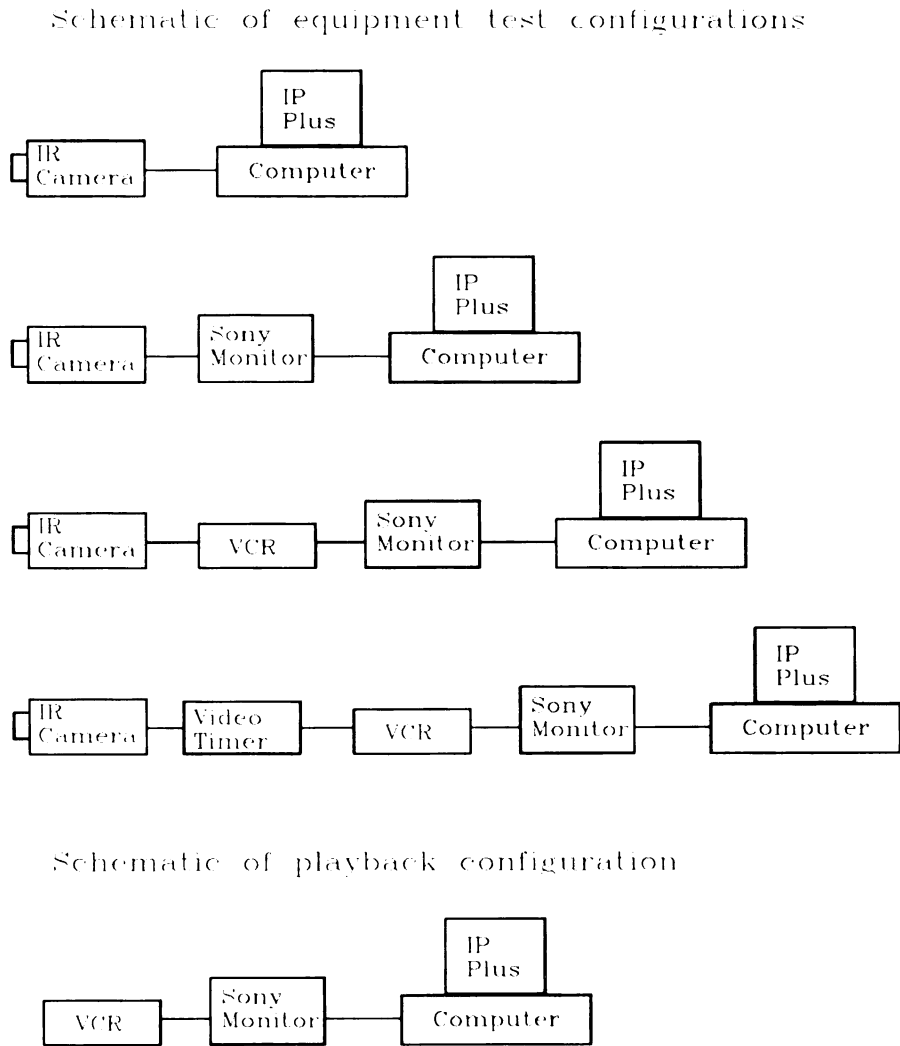


Figure 13. Schematic of the different equipment configurations tested.

The HP power supply was then adjusted to supply more electrical energy to the plate heater and the system was allowed to stabilize at a higher temperature. The IR camera was again used to measure the plate temperature with a variety of equipment configurations. Approximately 45 seconds were required to obtain data with each equipment configuration. Thus data with all of the different configurations could be obtained within 3 minutes. The temperature (as measured with the area function of the IR camera and a thermocouple) always remained stable during this time interval.

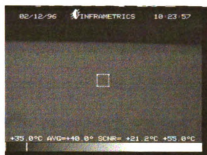
This process was repeated at various points in the temperature range defined by the IR camera. Typically a minimum of five data points were taken within the Inframetrics camera temperature range. Temperature ranges of 5 and 10⁰C were utilized for the experiments presented here for convenience, any of the camera temperature ranges could have been utilized. Typical images are shown in Figure 14.



a. 36.5°C



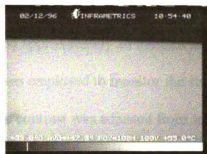
b. 37.7°C



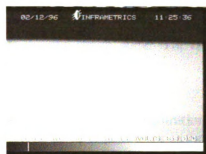
c. 40.0°C



d. 43.1°C



e. 47.3°C



f. 50.4°C

Figure 14. Playback data image sequence from the equipment test experiment conducted on 2/11/97.

3.3.2 BRIGHTNESS AND CONTRAST TESTS

The image processing software has three settings that affect how data are captured and imported: the brightness, contrast and gamma functions. The gamma function affects the linearity of the gray scale as a function of temperature. The gamma function was set at 1.0 and not adjusted since a linear curve was desired to maintain uniform sensitivity over the complete range. The brightness setting affects the y-intercept of the gray scale as a function of temperature. The contrast setting affects the slope.

The HP power supply was again used to raise the temperature of the plate heater from 5 to 10 °C above ambient temperature. The Inframetrics camera was set with the lower temperature range limit just below the temperature of the plate heater. The system was allowed approximately 20 minutes to come to thermal steady state. The IR camera area tool was employed to monitor the stability of the plate temperature.

The contrast was adjusted from settings of 65 to 100 (or until saturation occurred) with the brightness set at a fixed level. Brightness settings of 48, 50, 55, and 65 were selected for testing. These brightness test levels were chosen because settings above 65 caused saturation almost immediately and brightness settings below 48 clipped 40% off the dynamic range.

Experiments were conducted primarily with the plate temperature near the lower temperature limit of the IR camera. This was primarily due the fact that the loss of sensitivity in the IR camera resulted from the upward offset of the RS-170 signal. Tests were run with the plate temperature near the upper limit of the Inframetrics camera's

temperature scale. Preliminary results were similar to the lower limit tests. Focus was then placed on the lower limit tests.

It is important to note that the thermal target was at steady state for both the equipment configuration and the brightness/contrast tests. It is expected that the results and conclusions of these experiments would also apply for transient experiments.

3.4 RESULTS

These experiments showed that the data acquisition and processing equipment available in the HTRL affected the data. This effect can be seen in Figure 15 as each piece of equipment was added to the data acquisition circuit the gray scale-temperature response changed. The only piece of equipment that did not effect the signal was the Sony PVM-1343MD Trinitron monitor. The For-A VTG-33 affected the data in different ways depending on the setting of the 75Ω switch on the back panel. This switch placed 75 ohms of impedance between the device and the data signal. The remainder of the equipment and processing software had definite affects on the data and thus, the results of any experiment conducted with the IR camera system.

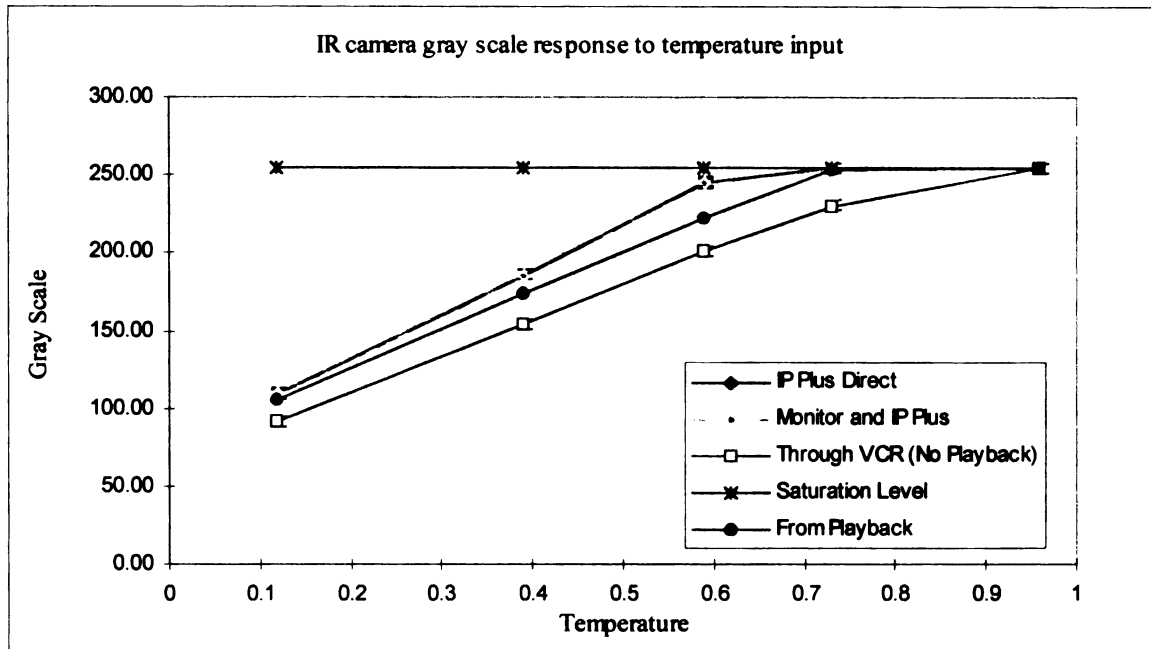


Figure 15. Equipment configuration effects on the IR camera gray scale-temperature response.

The results of each steady state test were compared to determine which equipment arrangement best matched the ideal system response defined in Figure 11. This ideal was defined to maximize the dynamic range of the IR camera and to maintain uniform sensitivity over the entire temperature measurement range.

It was found that the For-A VTG-33 Video Timer with the 75 ohm switch on did not affect the RS170 signal (Figure 16). The video timer allows time and date overlays to be placed on the data. This is highly desirable for transient tests, marking data with identification for later use, or time marking data for sequential information.

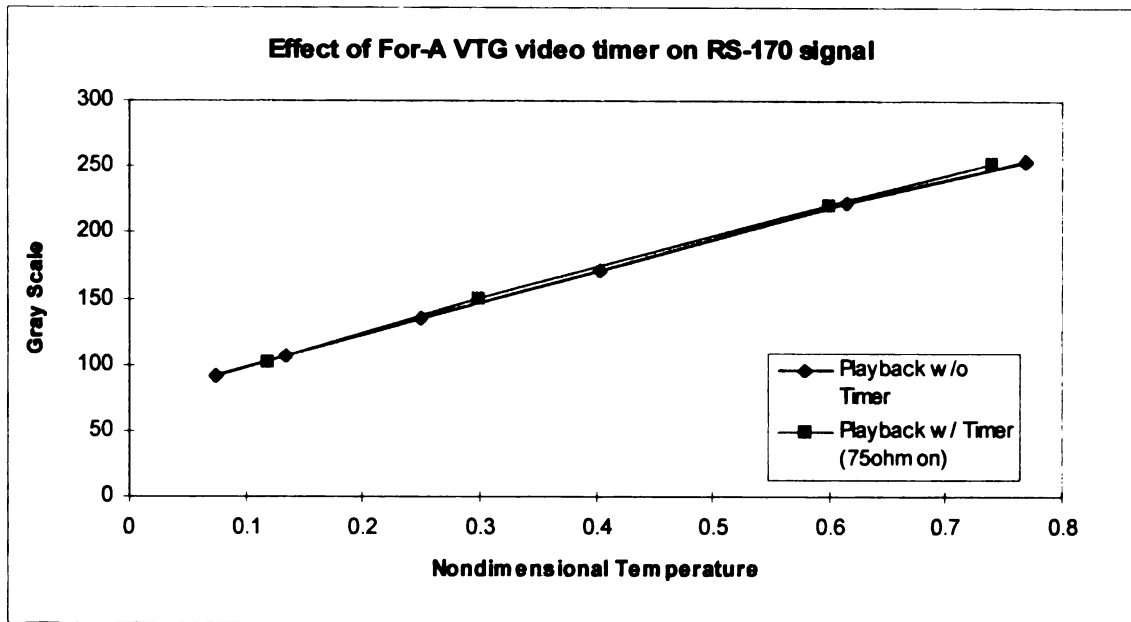


Figure 16. Comparison of equipment tests with and without the For-A VTG-33 video timer.

The Panasonic AG-2400 VCR did affect the RS170 signal and thus the gray scale to temperature relationship. Specifically, it created a negative offset on the RS-170 signal. This counteracted the positive offset from the camera and was necessary to capture the entire dynamic capabilities of the IR camera. The best results were obtained with the VCR in the data acquisition circuit but not recording the data stream. This arrangement would be possible during steady state tests, but is impractical due to the time required to process the data from a typical experiment with the Inframetrics camera.

Based on these results, the recommended equipment configuration for data acquisition is to connect the Inframetrics IR camera serially to the For-A VTG-33 Video Timer, to the Panasonic AG-2400 VCR, to the Sony PVM-1343MD Trinitron monitor (in that order).

The results of the brightness and contrast tests are shown in Figure 17. The brightness setting moved the overall curve upward, maintaining a constant slope. The contrast setting altered the slope of the resulting line. These settings appeared to operate independently of one another. These tests showed that the best settings to maximize the sensitivity were Brightness 48, Contrast 66. This setting was selected to lower the y-intercept of the gray scale as a function of temperature response. Figure 17 may make a contrast setting of 65 look like the best way to lower the response. However, this setting limited the upper response to a gray scale value of approximately 150 (thus sacrificing a large portion of the dynamic range). Based on these results, the optimal data processing system to achieve the ideal response shown in Figure 11, is the Panasonic AG-2400 VCR connected to the Sony PVM-1343MD monitor to the Image Pro Plus software (Figure 13).

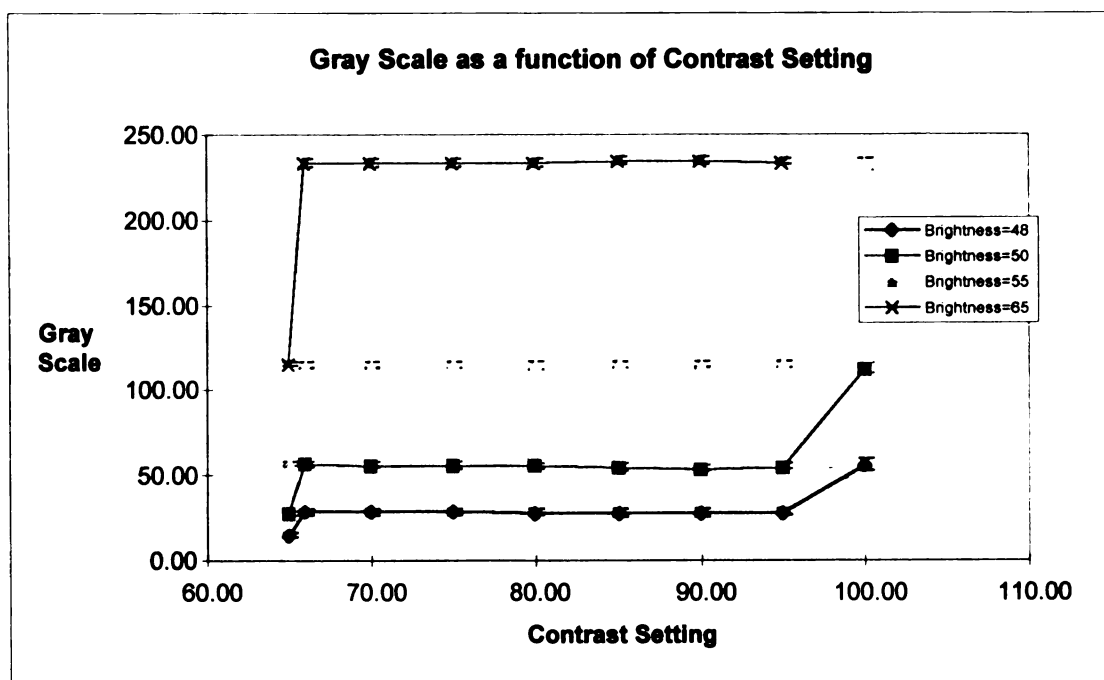


Figure 17. IR camera gray scale output as a function of contrast setting.
(Low end of Inframetrics camera temperature scale).

3.5 OPTIMAL CONFIGURATION TESTING

An optimal data recording system and a data playback system were defined from the results discussed above. The data recording system consisted of the Inframetrics IR camera connected to the For-A VTG-33 Video Timer and the Panasonic AG-2400 VCR (in that order). The data playback system consisted of the Panasonic AG-2400 VCR connected to the Sony PVM-1343MD Trinitron monitor with the signal then fed to the Image Pro Plus software (Figure 13).

This optimal equipment configuration was then tested. The test procedure was altered to reduce the time required. The plate was powered with the HP-6236B Triple output Power Supply to approximately 10 degrees above ambient. The plate was allowed 20 minutes to stabilize thermally. During these experiments, the temperature range of the Inframetrics IR camera was adjusted instead of changing the plate temperature. This procedure had the same effect on the IR sensor as adjusting the plate thermally. Several verification tests were run to insure that the results were identical for each procedure. This modified test procedure allowed for many more data points to be taken throughout the temperature range. This procedure allowed verification of the linearity of the Inframetrics IR camera output.

3.6 RESULTS OF OPTIMIZED EQUIPMENT CONFIGURATION

Previous work (White [1996]) had shown linear gray scale response to temperature but with a different slope and concluded that the offset was a characteristic of the radiometer itself. This previous study did not incorporate the affects of the contrast and brightness settings of the Image Pro Plus software which allow the offset to be

adjusted. Figure 18 and Figure 19 show the IR system response with optimal brightness and contrast settings and a comparison to previous calibrations obtained without these controls.

The equations in the upper corner of Figure 18 show the system insensitivity to contrast settings between 66 and 70. The correlation coefficient (R^2) values show the degree of linearity. The x-axis of these plots is presented in terms of non-dimensional temperature (T^*) which is defined as

$$T^* = \frac{T - T(\text{lower IR range limit})}{\text{IR camera Range (i.e. } 10^0 \text{ C)}} \quad (5)$$

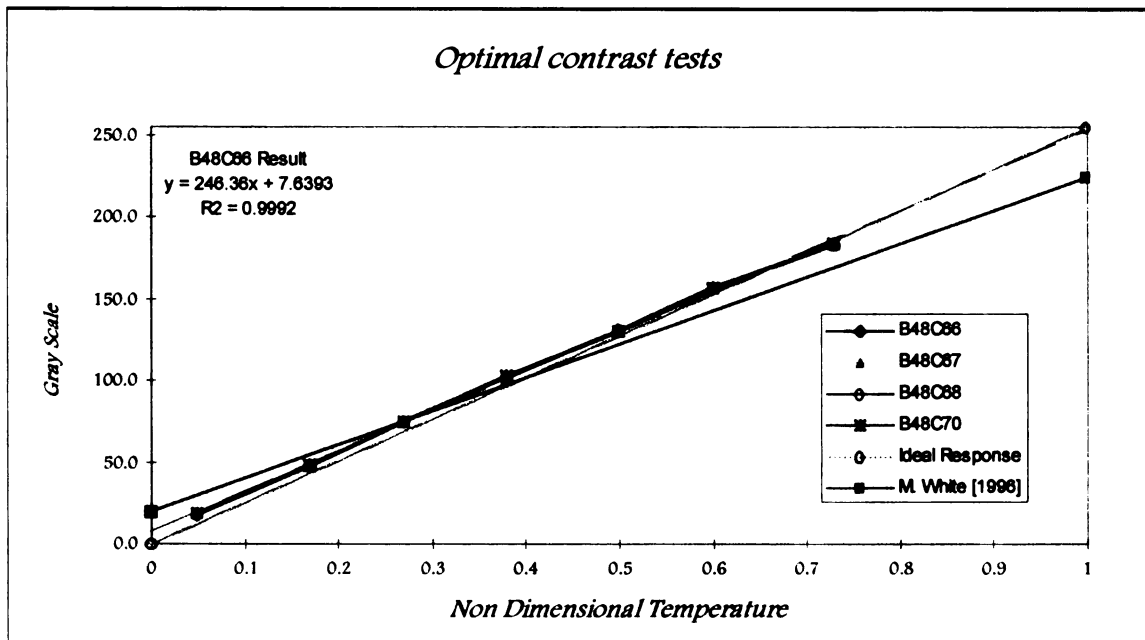


Figure 18. Gray scale-temperature relationship with optimal contrast.

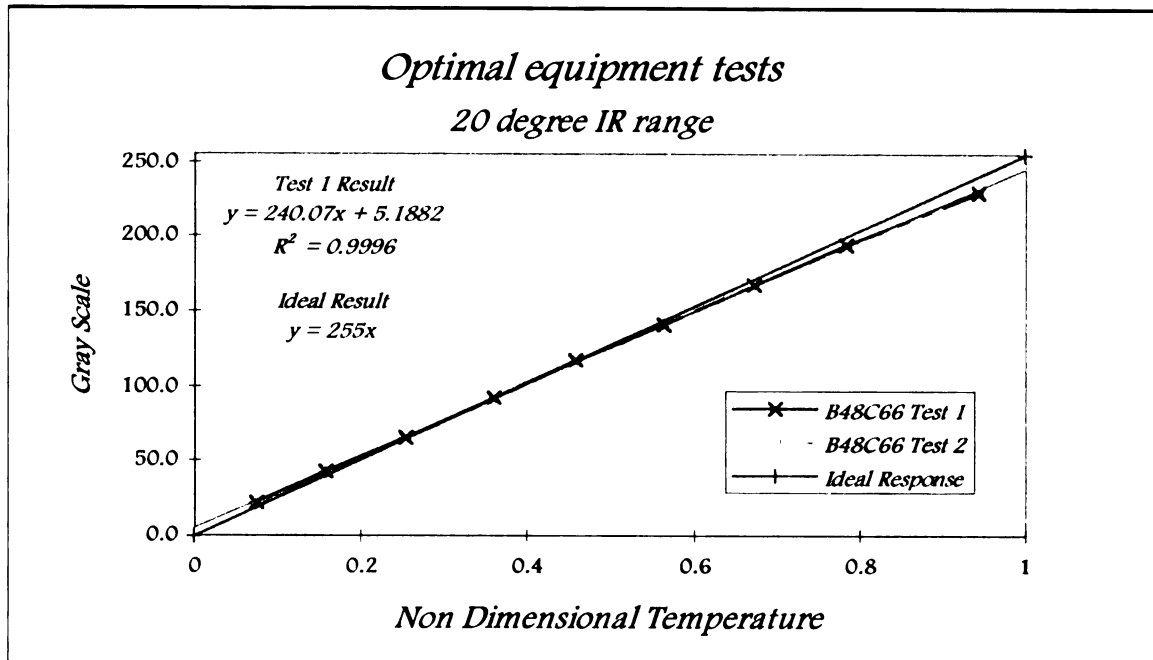


Figure 19. Optimal equipment configuration gray scale-temperature relationship.

The system response,

$$\text{Gray Scale} = 245.5 \cdot T^* + 7.7, \quad (6)$$

is almost identical to the optimal system response defined at the beginning of the investigation. The ideal response includes 100% of the dynamic range over the entire temperature scale. The optimized equipment configuration response is linear and provides 95% of the dynamic range for experimental work.

The results presented here should also be considered typical for any range setting on the IR camera but the specific experimental configuration should be characterized prior to each experimental sequence with the relevant equipment. The procedure described can be run in a reasonably short time frame and will help remove bias error created by the data acquisition system.

CHAPTER 4. SLIT RESPONSE FUNCTION - THEORY AND EXPERIMENTAL DERIVATION

4.1 INTRODUCTION

The Slit Response Function (SRF) is a measure of the ability of an infrared system to sense radiation from targets that subtend an angle which is smaller than the measurement resolution. An observable target smaller than the measurement resolution will produce a data signal that is attenuated as a function of target size. The SRF must be known so that these signals can be processed correctly and accurate measurements obtained. The lower thermal and optical measurement limits of the system can be defined if the SRF is known and corrections can be applied.

The instantaneous field of view (IFOV) and the field of view (FOV) are important factors in determining system performance. Generally a large field of view is desired with a small instantaneous field of view. The field of view is the total area the camera can sense and the instantaneous field of view is the projected detector area (Figure 20). As an analogy to a digitized image, consider the field of view the number of pixels and the instantaneous field of view as the pixel size.

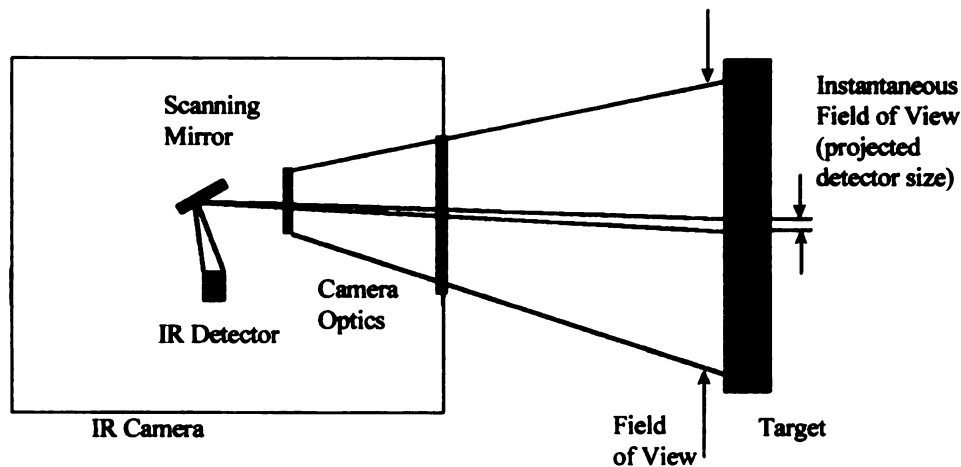


Figure 20. Schematic of IR camera optical configuration and definition of terms.

Scanning infrared systems tend to have different SRFs in the scan and cross scan directions due to factors such as detector size and shape, line to line interpolation schemes, optics and scan rates. The SRF for a given system defines the limits on imaging and measurement resolution. The optical (imaging) resolution is typically defined as the target angle that will produce a 50% response (that is, it will measure 50% of the full scale temperature above or below background). The measurement resolution is defined as a target width that will produce a 99% response (Holst [1993]). The measurement resolution defines the smallest target angle that may be thermally measured accurately.

The effects of the scanning direction and target alignment can be seen in Figure 21, Figure 22 and Figure 23. The scan direction is from left to right. The MAF sensor is at the same temperature for both images ($T \sim 56^{\circ}\text{C}$). The sensor aligned with its narrow dimension in the scan direction did not produce as large a response as the sensor aligned with the scan direction.

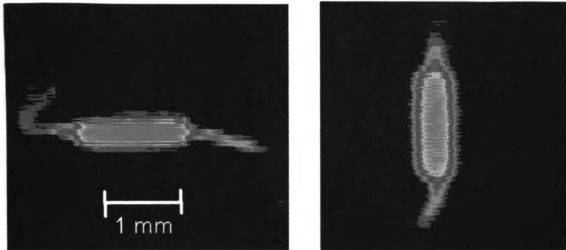


Figure 21. Comparison of scan direction effect on IR camera response.

The MAF sensor alignment with respect to the scan direction affects the length of time that the infrared detector has to respond to the radiation emitted. Figure 22 shows a much flatter response to the target than Figure 23. This is because the SRF is created by step changes or steep gradients in the emitted radiation. When the sensor is aligned with the scan direction, its long dimension allows the infrared detector more time to equilibrate. Therefore, the scan direction defines the critical dimension related to accurately measuring temperature and was the focus of the study.

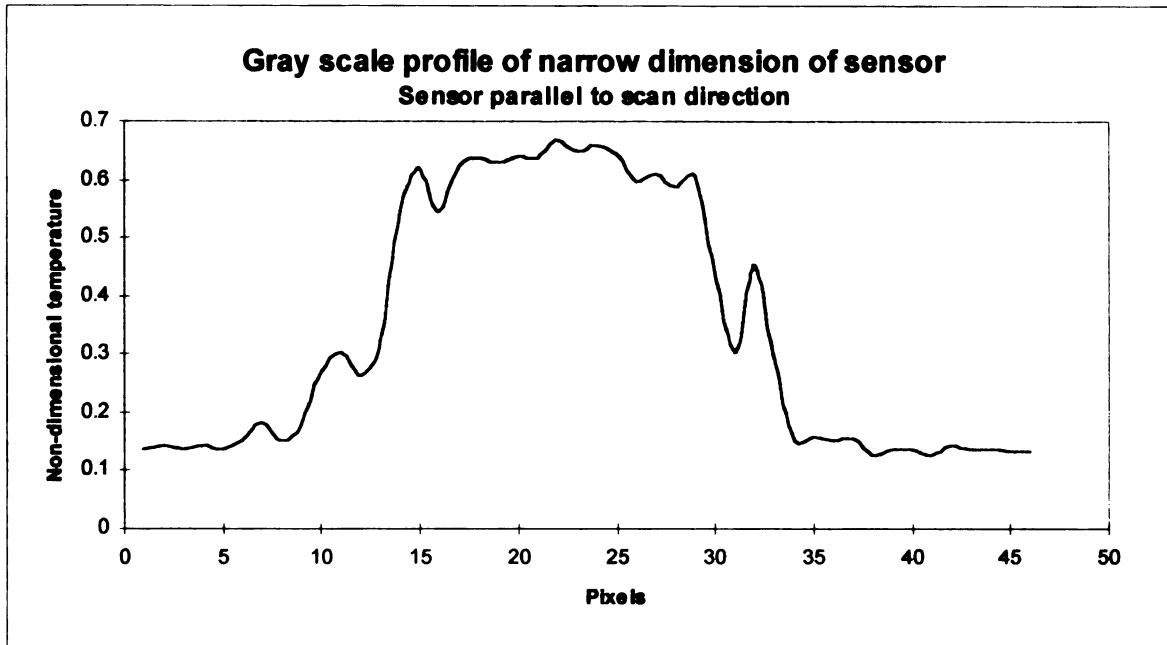


Figure 22. Temperature profile of narrow dimension of the MAF sensor.
Sensor parallel to scan direction.

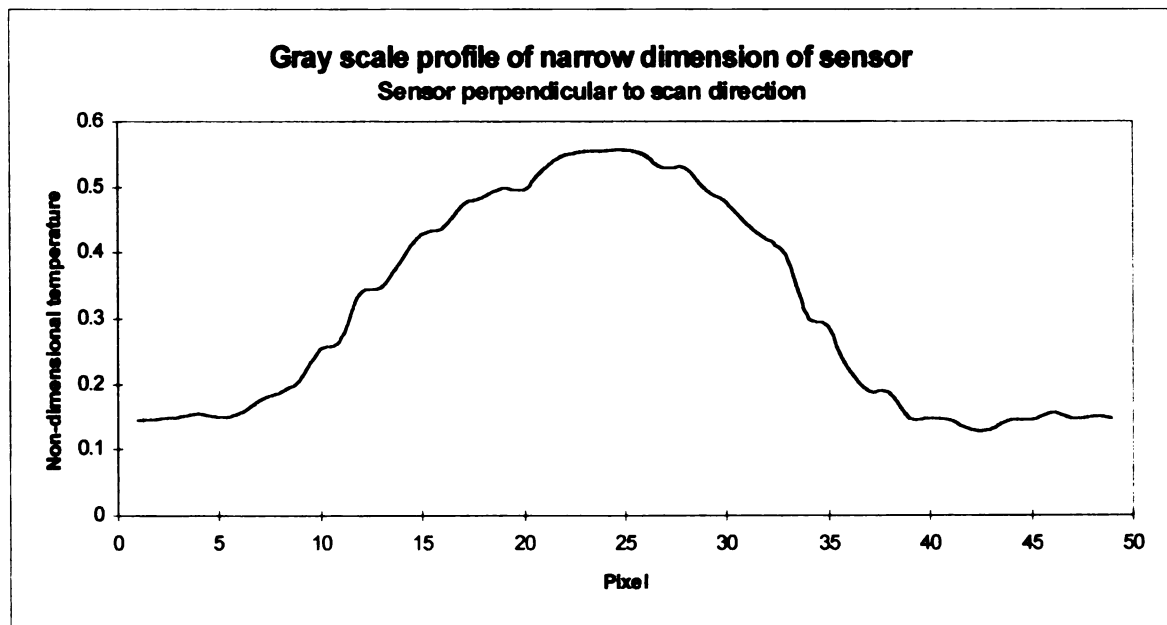


Figure 23. Temperature profile of sensor narrow dimension.
Sensor perpendicular to scan direction.

The slit response function for the 600L Inframetrics IR camera was determined experimentally. An anticipated SRF response can be calculated from

$$\Delta E_{sys} = \left[G \int_{\lambda_1}^{\lambda_2} R(\lambda) \frac{\Delta L_e(\lambda, T) A_o A_{IFOV}}{(f_{col})^2} T_{sys}(\lambda) T_{test}(\lambda) d\lambda \right] ATF_{sls}. \quad (7)$$

However since this equation utilizes other measured characteristics of the IR system and the target (i.e. the Aperiodic Transfer Function (ATF) and the spectral emittance), it is more useful and much simpler to determine the SRF experimentally. Experimental determination also accounts for issues such as clouded or misaligned lenses

4.2 IMAGE PROCESSING EFFECTS ON DATA

The Inframetrics 600L camera has a field of view of 20° horizontal x 15° vertical (0.34907 x 0.26180 radians) (Inframetrics [1994]). There are 175 instantaneous fields of view (IFOV) per line and 131 lines vertical lines that comprise the entire field of view (FOV). The electronics sample 256 times per line (1.46 samples per IFOV). These data are output in an analog RS-170 signal in U.S television format. The RS-170 signal has 525 lines which are interlaced so that there are approximately 240 real lines of data. The other lines are used by synchronization signals and repositioning of the scanner (Russ [1995]). The original 175 IFOV x 131 lines of optical samples are now divided into 256 x 232 data bins. The signal was then acquired by the digital frame grabber board and split again into 640 x 480 discrete pieces of information (pixels). Each IFOV was now spread across 3.66 digital pixels. Each of the 256 data samples per line was divided into 2.5 pixels horizontally and each vertical line of data was spread over two lines of digital pixels

and interlaced. Although no information was lost, it was converted to analog and resampled into a different number of information packets as it was processed.

4.3 EXPERIMENTAL TEST PROCEDURE

The procedure to determine the SRF experimentally was taken from Testing and Evaluation of Infrared Systems by Holst [Holst 1993]. The test consists of utilizing a micrometer traverse system to manipulate a mechanical slit. The slit is placed between the IR camera and the blackbody source (Figure 24). The IR camera is focused on the edges of the slit to capture collimated (parallel) IR radiation emitted from the source. The slit now appears as a target source to the system. The mechanical slit is closed so that the zero position is known and then opened in incremental steps and the response of the IR system is recorded. It is important to insure that one measurement is taken of the full scale (unobstructed) view of the blackbody to non-dimensionalize the results.

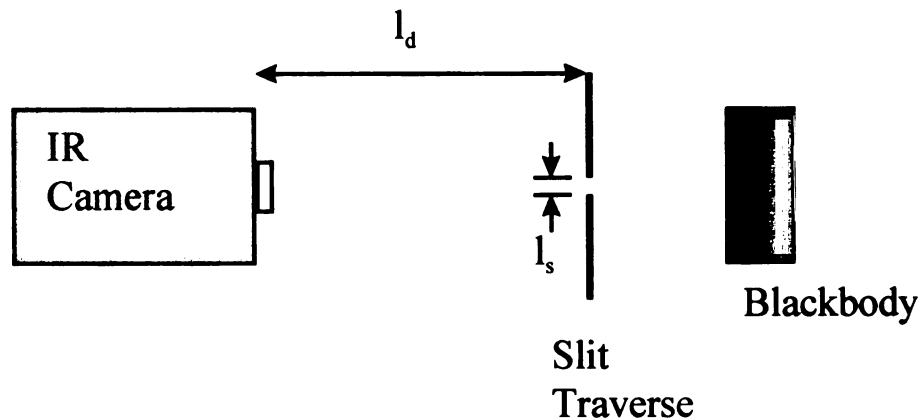


Figure 24. Schematic of the experimental configuration for SRF measurement.

It is crucial to maintain a large enough distance between the blackbody and the slit to prevent radiative heating of the slit. A 3" gap between the heated plate and the mechanical slit was utilized for this study and the back of the slit was made of polished aluminum to further reduce thermal absorption. A change in the slit mechanism temperature has the effect of changing the temperature step that the sensor must track and will seriously affect the results. This is also why it is critical to maintain the blackbody at a constant temperature.

A blackened 3" diameter aluminum plate thermally bonded to an Omegalux silicone rubber electric heater acted as the blackbody source for the experiments. The emissivity of the plate has been measured previously as 0.95 utilizing the temperature comparison method (Inframetrics [1988]). The actual emissivity and temperature of the thermal source are not critical to this experiment. However, they must be stable.

The internal focal distance of the IR camera must be accounted for to properly calculate the viewing angle. The target angle Θ is defined as

$$\Theta = \tan^{-1} \left(\frac{l_s}{(l_d + l_i)} \right). \quad (8)$$

The distance l_s is the target width in the scanning direction. The distance from the target to the bayonet mount lens on the IR camera is l_d . The internal focal path length of the camera is l_i . The Inframetrics 600L camera has an l_i of 260.4mm. The non-dimensionalized system response can then be utilized to calculate the target temperature for any target at any distance from the IR camera assuming the target emissivity and target size are known.

4.4 RESULTS

The SRF for the Inframetrics 600L camera with no external optics is shown in Figure 25. The error bars show the 95% confidence region determined from the experimental data. It can be seen that the uncertainty increases significantly at smaller angles. Figure 26 shows the 95% confidence region divided by the mean SRF value. This plot defines resolution limits if predictive capabilities of the system are considered.

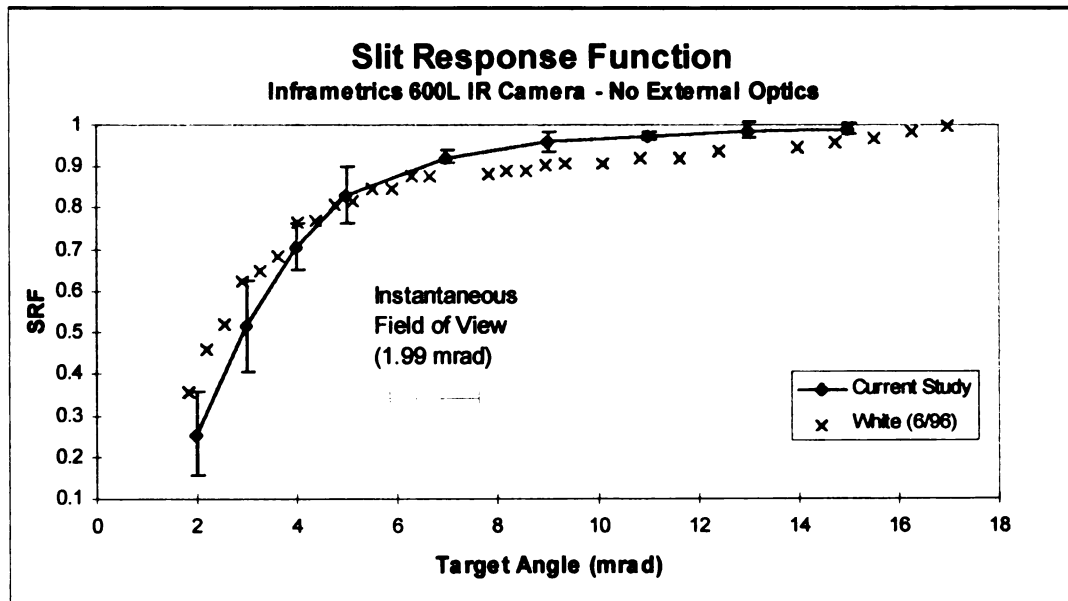


Figure 25. Slit response function with 95% confidence region (n=5) for the Inframetrics 600L IR camera.

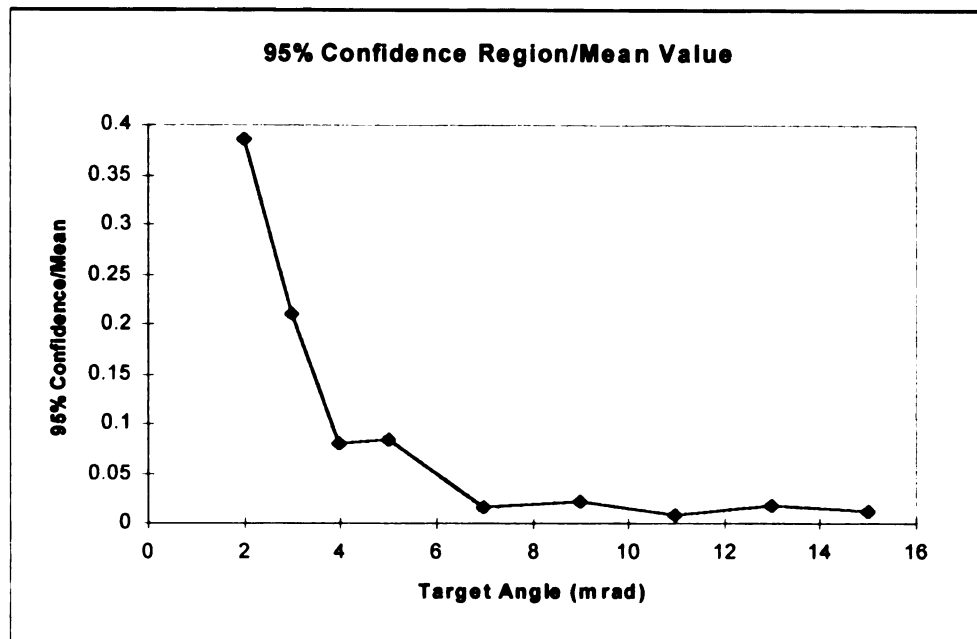


Figure 26. SRF confidence region/mean value for Inframetrics 600L IR camera with no external optics.

The HTRL also has a 3x telescopic lens with a 6" close up attachment for working with smaller samples. The SRF of this configuration was also determined experimentally and is shown in Figure 27. The figure also shows the 95% confidence regions. This lens has only one working distance, so target width and target angle are interchangeable (since l_d and l_i are not adjustable). The internal focal length (l_i) is different than in the previous case without the external lenses. The sum of the internal focal length and the working distance is equal to 77 mm for this arrangement. The actual working length is 145mm, the decrease is a result of the magnification factors of the lenses. Due to this complexity, the results are presented as a function of target width instead of target angle.

Figure 25 and Figure 27 both show data obtained by White (White [1996]) with the same equipment in the same laboratory. White used only a single data set and the IR camera system was not optimized in the same manner described in this document. For

example, in Figure 27, White's data levels out at 0.1. This is indicative of either a poor calibration or heating of the slit. However, White's data show similar trends and are presented for completeness of the work on this infrared system.

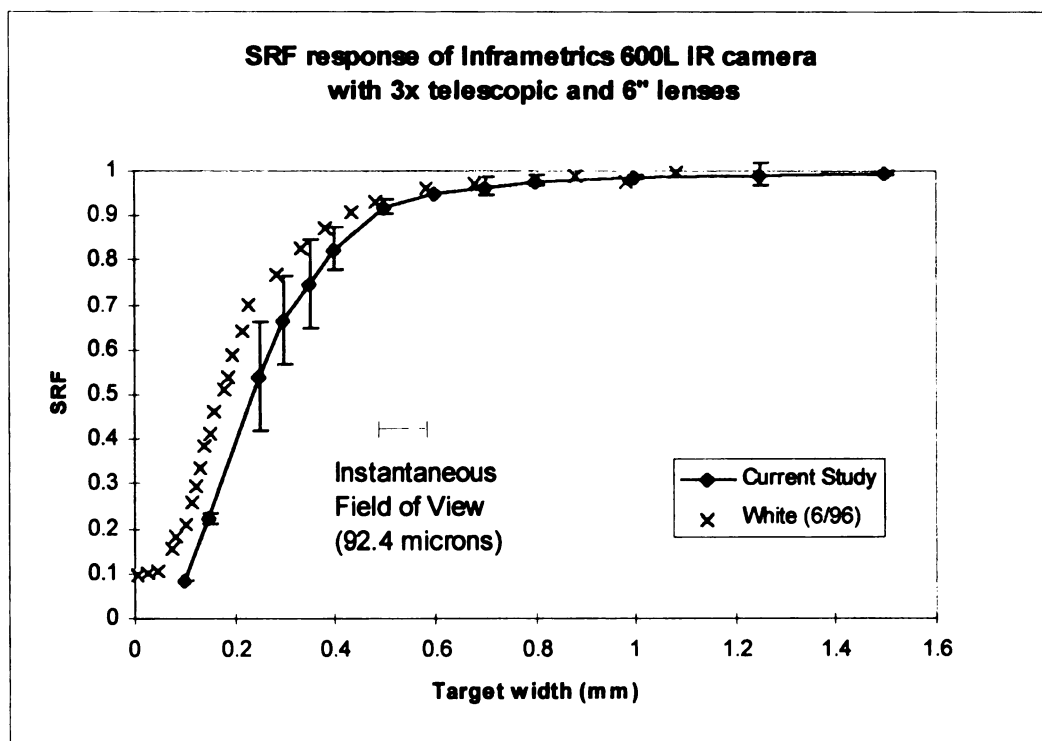


Figure 27. SRF of the Inframetrics 600L infrared camera with 3x Telescopic and 6" close-up lenses.

Inframetrics specifies that the 50% SRF corresponds to 0.002 radians for this system when it was manufactured. The system currently has a 50% SRF at 0.00291 radians (Figure 25). There are several possible explanations for this variation. The system is due to be calibrated and it may require that the internal optics be cleaned. Also, the scanning mirror and the IR detector may be slightly misaligned according to Inframetrics technical support staff.

4.5 PREDICTIVE CAPABILITIES

The data obtained allows for temperature measurements to be obtained from targets smaller than the measurement resolution of the system. The data also allows for an understanding of the general capabilities of the infrared system and its limitations so that experiments can be properly designed. Small targets can be measured thermally with an understanding of the accuracy of the measurement and experiments can be designed to avoid resolution issues. Most importantly, a general understanding of infrared thermal measurement techniques can be obtained so that the equipment can be used properly.

The following example will illustrate how to utilize the IR camera for an unresolved target. Figure 28 shows a pseudo-colored infrared image of an electrically heated MAF sensor taken with the Inframetrics 600L IR camera operating with the 3x telescopic and the 6" close-up lenses. The sensor has dimensions of 1.5 mm long by 0.5 mm wide.

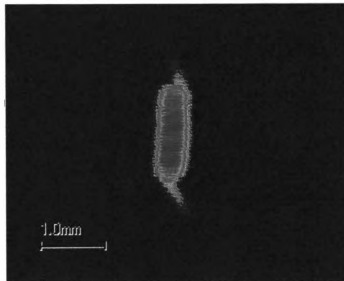


Figure 28. Thermographic image of MAF sensor.

Figure 27 shows that 0.5mm is not large enough for the Inframetrics camera to have a full scale response. The IR system will produce a 90% percent response with a 3% uncertainty at a 95% confidence level.

The gray scale response of the camera is related to the temperature measured as shown in Chapter 3. The system has been calibrated so that a known linear relationship exists between gray scale and temperature as shown in

$$T = \frac{\text{Gray Scale} - 7.6}{246} * T_{\text{range}} + T_{\text{Lower Limit}} . \quad (9)$$

Note that this relationship was obtained with specific equipment and the relationship should be determined for each particular configuration. The variable T_{range} is the temperature range setting on the IR camera (i.e. 10⁰C) and $T_{\text{Lower Limit}}$ is the base of that range (i.e. 40⁰C for a range of 40-50⁰C).

Consider that the camera measures a gray scale reading of 100 (out of 256) on a target with an SRF of 66% and an uncertainty of 9% at a 95% confidence level. If the temperature measurement scale was set on 40-50 ⁰C, this would be equivalent to measuring 43.9 ⁰C using Equation 9. The correct gray scale value and uncertainty in that value can be found from

$$\text{Gray Scale}_{\text{Actual}} = \frac{\text{Grey Scale}_{\text{measured}}}{\text{SRF}} \quad (10)$$

and

$$\Delta \text{Gray Scale}_{\text{uncertainty}} = \frac{\text{Gray Scale}_{\text{Measured}} \pm \% \text{Uncertainty}}{\text{SRF}} \quad (11)$$

$$\% \text{Uncertainty} = 95\% \text{ confidence range}$$

respectively. This would result in a gray scale reading of 152 or 45.9°C and 95 % confidence gray scale limits of 137 - 164 (45.4- 46.4°C) for this example.

The resolution decreases linearly with increasing temperature range settings of the camera. Consider the previous example but with the temperature range set at 50°C (30-80 °C for example). A gray scale reading of 100 would correspond to a temperature of 48.0 °C (again, using Equation 9). The corrected gray scale value would be 152 as before but this would result in a temperature of 58.2 °C with a 95% confidence range from 56.0 - 64.3 °C.

It appears logical to use the smallest temperature range possible to reduce the range and thus reduce the error. However, it is essential that the full scale reading and the attenuated reading be contained in the IR camera range setting for this procedure to function optimally.

Experiments were conducted to investigate the predictive capabilities when the target temperature exceeded the range setting on the infrared camera. The experimental conditions included a target angle of 0.002 radians and the camera temperature range set 10-20 degrees below the target temperature and not encompassing the target temperature. These experiments showed that the system was unable to reliably predict the correct temperature utilizing the SRF data presented here. It is therefore recommended that the temperature scale on the IR camera be set in such a way that the temperature of the target is incorporated in the range.

4.6 CONCLUSIONS

A universal curve for the Inframetrics 600L IR camera was obtained (Figure 29). This information specifies the response of the system and the uncertainty associated with the measurement obtained. Proper non-dimensionalization requires that the working distance and the internal focal length be utilized. The sum of the working distance and the internal focal length ($l_i + l_d$) for the system with the 3x telescopic lens and the 6" close-up optics is equal to 77mm. The internal focal distance for the system with no external optics is 260.4mm.

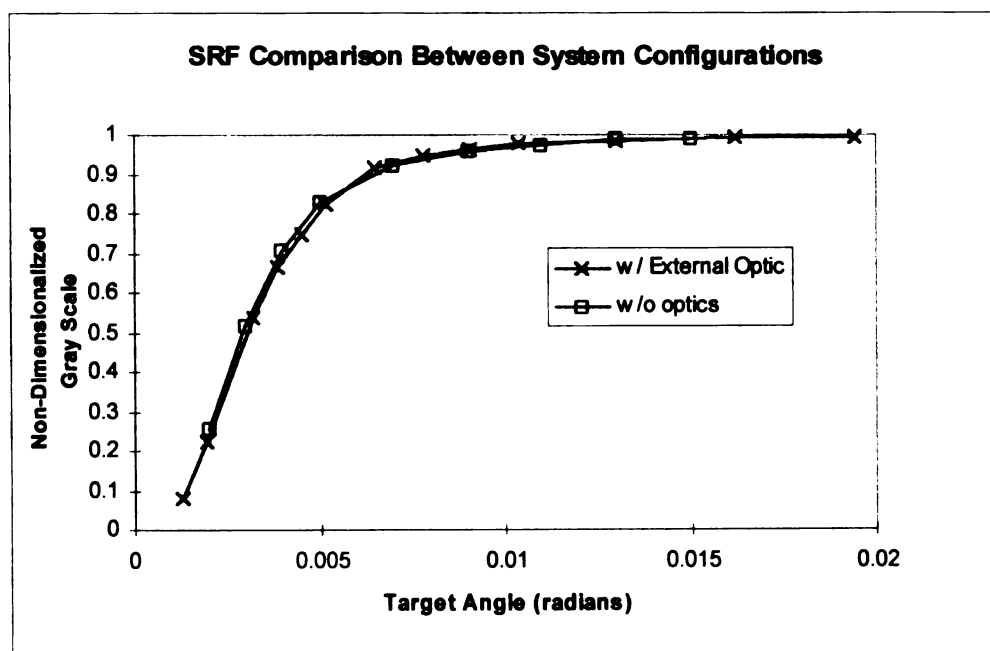


Figure 29. Comparison of SRF between system configurations (no optics compared to external optics).

Dimensions in the scan direction are specified in Table 1 for the optical resolution (50% detector response) and the measurement resolution (95% detector response). Recall that for the system with external optics, the working distance is fixed at 14.5cm from the

external lens. Uncertainty ranges can be obtained from the 95% confidence regions shown in Figure 25 and Figure 27.

Table 1. SRF summary for the Inframetrics 600L infrared camera in the HTRL.

Slit Response	Target Information (no external optics)		Target Information (w/ external optics)	
% Response	Angular (rad)	Width @ l_d	Angular (rad)	Width @ 14.5cm
50% Response (optical resolution)	0.00291	1.49mm @ 25cm 2.21mm @ 50cm	0.00291	0.224mm
99% Response (measurement resolution)	0.0105	5.36mm @ 25cm 7.98mm @ 50cm	0.0105	0.808mm

The information presented here should allow for the Inframetrics 600L camera to be utilized effectively to perform thermal measurements of targets as small as 25% of the measurement resolution. A substantial increase in measurement uncertainty will occur as the target becomes smaller and less visible to the camera sensor. Chapter 5 will show an experimental to confirm that these compensations can be realized for small objects.

CHAPTER 5. EXPERIMENTAL VERIFICATION OF THERMOGRAPHIC TEMPERATURE MEASUREMENT UTILIZING SLIT RESPONSE CORRECTION

5.1 INTRODUCTION

The procedure that will be outlined compensates for two separate variables that will affect the measurement accuracy of the infrared imaging system: the dimensions and emissivity of the target. The size of the target generally can be determined easily and accurately with either a mechanical measurement device (such as a micrometer) or optically using a calibrated reticule. Either of these methods are accurate enough for the study presented here. It is important to note that if the thermographic instrument is capable of large magnification values, the measurement of the target dimensions becomes more critical. The target emissivity will be determined as part of the procedure.

5.2 EXPERIMENTAL PROCEDURE

The following procedure was utilized to measure the target dimensions and emissivity so that general experimental measurements could then be taken:

1. Measure target dimensions.
2. Position target at $X/D=0.5$ under the calibration nozzle (position a calibrated thermocouple below the target to monitor flow temperature).
3. Fill Inframetrics 600L infrared camera dewar with liquid nitrogen, turn the camera on and run for 20 minutes. Refill the dewar.
4. Position Inframetrics 600L infrared camera inside the sub atmospheric chamber so that the target is in focus. Measure the distance between the infrared camera and the target. Refer to Figures 25 and 27 to determine SRF value and uncertainty.

5. Seal the wind tunnel. Turn on the prime mover and set the sluice gate so that there is a pressure differential (measured with the MKS Baratron pressure transducer) of approximately 0.241 in-H₂O across the calibration nozzle (This corresponds to flow velocity of approximately 10 m/s).
6. Turn on the HP6274B DC power supply to provide 8 amps of electrical current to the flow heater (this corresponds to a flow temperature of approximately 56⁰C, depending on the ambient temperature).
7. Allow the system to equilibrate for approximately 20 minutes.
8. Determine the target emissivity (ϵ).

- a. The flow temperature is measured with a calibrated thermocouple. Calculate the gray-scale value from the infrared camera that will produce the flow temperature using

$$Gray\ Scale = \left(\frac{T_{flow} - T_{Range - Min}}{T_{Range}} \right) \cdot SRF \cdot 256 \quad (12)$$

for the ideal response. If the system was calibrated (Chapter 3), use the appropriate transfer function such as

$$Gray\ Scale = \left(\frac{T_{flow} - T_{Range - Min}}{T_{Range}} \right) \cdot SRF \cdot 240.07 + 8.19 \quad (13)$$

for the 20⁰C calibration.

- b. Adjust the camera emissivity setting until the gray-scale output matches the value calculated in step 8a.

9. Adjust the HP6274B DC power supply to provide 6 amps of electrical current to the flow heater (this corresponds to a flow temperature of approximately 36⁰C, depending on the ambient temperature).
10. Repeat step 8 as a verification of the emissivity.
11. The target can now be placed in any environment (for example, its operating conditions) and its temperature can be determined (within the uncertainty specified in the Figure 25 or 27 appropriately).

5.3 EMISSIVITY MEASUREMENT

The target emissivity can be determined by two different methods. The first is a procedure that is outlined in the Inframetrics 600L operator's manual (Inframetrics [1988]). This method requires measuring the energy from two different thermal sources (source A and source B) directly and reflected off the test specimen. The reflectance (ρ) can be calculated from this information using

$$\rho = \frac{\text{Source A Refected Level} - \text{Source B Reflected Level}}{\text{Source A Direct Level} - \text{Source B Direct Level}}. \quad (14)$$

The target emissivity can then be calculated from a simple energy balance such as

$$Q_R = (\alpha + \tau + \rho) \cdot Q_R \Rightarrow \alpha + \tau + \rho = 1. \quad (15)$$

The energy incident on the target (Q_R) must either be absorbed (α), transmitted (τ) or reflected (ρ). This is further reduced to

$$\varepsilon = 1 - \rho \quad (16)$$

if the target is opaque (its transmissivity (τ) is equal to zero) and the gray body assumption of $\alpha = \varepsilon$ (Kirchoff's law) (Weast [1986]) is applied.

This method can be difficult to implement. Difficulty arises from three requirements of the method. The reflection of the two reference sources must be viewed on the test specimen. The reflection dimensions must be known if the slit response function correction is to be applied. The reflection can be very difficult to measure accurately. Finally, if the test specimen has a high emittance (absorptivity) (>0.8) obtaining a reflection that can be imaged clearly is almost impossible unless very high temperature reference sources are utilized.

The second method, which was employed in this study and included in step 8 of the procedure in section 5.2, was to place the target in an environment such that its temperature was known. The dimensions of the target must be known prior to the application of this method because the unresolved target requires the SRF correction to measure temperature. The isothermal environment was obtained by using the calibration nozzle and the electric flow heater (Chapter 2, section 2.9) to provide a jet flow with a known, uniform temperature profile (within ± 1.5 °C). It is important to raise the target temperature above ambient to increase the ratio of emitted radiation to reflected radiation (effectively, the signal to noise ratio). The target temperature can then be measured directly with the infrared camera (with the slit response function correction applied). The emissivity setting on the camera can then be manipulated until the gray scale output matches the calculation from the appropriate transfer function. It is important to note that although the infrared imaging system was calibrated previously (Chapter 3), new software and a new VCR were utilized during the experimental verification. The addition of the new equipment allowed for the ideal response (Equation 12) to be realized and thus Equation 12 was utilized throughout this chapter.

It is critical to use the SRF correction to accurately measure the emissivity. An ‘apparent’ emissivity will be measured without the SRF correction. This restricts the experimental configuration to the original working distance (Gartenberg and Roberts [1990]). Any deviation from this working distance will cause the ‘apparent’ emissivity to change and introduce systematic errors to the measurements.

5.4 EXPERIMENTAL VERIFICATION

Two experimental procedures were conducted. The first procedure utilized the MAF sensor shown in Figure 28. This target required that the external optics were utilized and produced an SRF value of 0.9. The second target was a metal cylinder (painted black) with a diameter of 1.75 mm. The IR camera was positioned 34 cm away from the target and the external optics were not utilized. This produced a target with an SRF of 0.57. The cylinder could have been viewed from closer or with the external optics to obtain a well resolved target. However the test was conducted to investigate the SRF correction.

In the first procedure, the MAF sensor was mounted below the calibration nozzle in the HTRL facility and the procedure in section 5.2 was followed through step 8. The IR camera emissivity setting was adjusted, an image was acquired and processed, and the target temperature was calculated from Equation 12. This procedure was followed until the target temperature matched (approximately) the flow temperature measured by the calibrated thermocouple. This required processing each data point prior to proceeding. Six data points were taken with the final emissivity setting. Each thermographic image was

the average of 16 frames to reduce the effects of noise. The results of the emittance determination are shown in Table 2.

Table 2. Emissivity measurement results ($\epsilon=0.88$).

	Measured Gray Scale	SRF Corrected Gray Scale	SRF Corrected Temperature ($^{\circ}\text{C}$) (Equation 12)
Test 1	225	250	49.6
Test2	238	264.4	50.8
Test 3	240	266.7	50.9
Test 4	225	250	49.6
Test 5	226	251.1	49.7
Test 6	223	247.8	49.5
Mean	229.5	255	50.0
Variability (95% confidence level)	14.6	16.2	± 1.58
Thermocouple measurement data			$49.6 \pm 2.8^{\circ}\text{C}$ (95% confidence)

The SRF corrected gray scale values averaged 255 and some values exceeded the 255 limit of the 8-bit scale. Section 4.5 warned about the possibility of introducing error by extrapolating temperatures beyond the IR temperature range setting (or gray scale values greater than 255). The gray scale - temperature relationship is assumed to be a linear relationship in this analysis. This relationship potentially becomes non-linear beyond the IR camera range setting. Preliminary experiments showed that the temperature calculation became less reliable if temperatures beyond the infrared camera temperature

range were extrapolated. That affect may be present in these validation experiments as a decrease in the predictive accuracy and an increase in the standard deviation.

The variability presented in all of the tables in this chapter are the experimental variance (L) defined at a 95% confidence level with

$$L = \sqrt{\frac{4t^2 \hat{\sigma}^2}{n}}, \quad (17)$$

where n is the number of data points, σ is the sample standard deviation and t is the variable from the Student's t statistic.

The power to the flow heater above the calibration nozzle was then set to two different levels to simulate unknown operating conditions. A calibrated thermocouple was utilized to monitor the flow conditions. The results of tests 1a and 1b are shown in Table 3 and Table 4 respectively.

Table 3. Test results from test 1a (MAF sensor)
(11 amps to flow heater, 42.1 - 62.1⁰C IR temperature range).

	Measured Gray Scale	SRF Corrected Gray Scale	SRF Corrected Temperature (⁰ C) (Equation 12)
Test 1	253	281.1	64.1
Test 2	211	234.4	60.4
Test 3	159	176.7	55.9
Test 4	197	218.9	59.2
Test 5	252	280	64.0
Test 6	215	238.9	60.8
Test 7	190	211.1	58.6
Test 8	209	232.2	60.2
Test 9	232	257.8	62.2
Test 10	219	243.3	61.1
Test 11	222	246.7	61.4
Test 12	250	277.8	63.8
Test 13	206	228.9	60.0
Mean	216.5	240.6	60.9
Variability (95% confidence level)	52.4	58.2	±5.1
Thermocouple measurement data			61.0 ± 3.4 ⁰ C (95% confidence)

Table 4. Test results from test 1b (MAF Sensor)
(4 amps to flow heater, 20.0 - 40.0°C IR temperature range).

	Measured Gray Scale	SRF Corrected Gray Scale	SRF Corrected Temperature (°C) (Equation 12)
Test 1	210	233.3	38.2
Test 2	191	212.2	36.6
Test 3	210	233.3	38.2
Test 4	229	254.4	39.9
Test 5	228	253.3	49.8
Test 6	181	201.1	35.7
Test 7	201	223.3	37.4
Test 8	225	250	39.5
Test 9	231	256.7	40.0
Test 10	203	225.6	37.6
Test 11	195	216.7	36.9
Test 12	223	247.8	39.4
Test 13	185	205.6	36.1
Test 14	229	254.4	38.1
Mean	208.6	231.8	38.1
Variability (95% confidence level)	33.0	36.6	±3.15
Thermocouple measurement data			36.6± 1.96°C (95% confidence)

The second experimental verification utilized the Inframetrics 600L infrared camera with no external optics. A metal cylinder with a 1.75 mm diameter was placed under the calibration nozzle in the HTRL facility and the procedure outlined in section 5.2 was executed. The cylinder was positioned 34 cm in front of the infrared camera. This created a target angle of 2.92 mrad and the resulting SRF was calculated from a curve fit from Figure 25 as 0.57.

The IR camera emissivity setting was adjusted, an image was acquired and processed, and the target temperature was calculated from Equation 12. This procedure was followed until the target temperature matched (approximately) the flow temperature measured by the calibrated thermocouple. This required processing each data point prior to proceeding. Six data points were taken with the final emissivity setting. Each thermographic image was the average of 16 frames to reduce the effects of noise. The results of the emittance determination are shown in Table 5.

Table 5. Emissivity measurement results ($\epsilon=0.95$).

	Measured Gray Scale	SRF Corrected Gray Scale	SRF Corrected Temperature ($^{\circ}\text{C}$) (Equation 12)
Test 1	218	382.5	55.8
Test2	217	380.7	55.6
Test 3	216	379.0	55.5
Test 4	212	371.9	55.0
Test 5	216	379.0	55.5
Test 6	237	415.8	58.4
Mean	219.3	384.8	56.0
Variability (95% confidence level)	17.43	30.58	± 2.9
Thermocouple measurement data			$55.4 \pm 1.7^{\circ}\text{C}$ (95% confidence)

The power to the flow heater was then adjusted to two different settings. The system was allowed to equilibrate and images were taken of the metal cylinder. Sixteen images were taken and averaged at every data point to reduce electronic noise. The results of the two experiments are shown in Tables 6 and 7.

Each of the experimental results of the temperature measurement (Tables 3,4,6 and 7) includes a different number of tests. This was due in part to images that were taken but were saturated and were discarded. The images were post processed and therefore saturation was not detected until after the experiment was over. Also, each test series ended when the IR camera displayed a “low liquid nitrogen” signal. This indicates that the

dewar required refilling and this effectively ended the test series because the IR camera was closed in the HTRL flow facility.

Table 6. Test results from test 2a
(11 amps to flow heater, 32.9 - 52.9°C IR temperature range).

	Measured Gray Scale	SRF Corrected Gray Scale	SRF Corrected Temperature (°C) (Equation 12)
Test 1	224	393.0	63.6
Test 2	213	373.7	62.09
Test 3	216	379.0	62.5
Test 4	223	391.2	63.5
Test 5	237	415.8	65.4
Test 6	238	417.5	65.5
Test 7	232	407.0	64.7
Test 8	228	400.0	64.2
Test 9	239	419.3	65.7
Test 10	239	419.3	65.7
Test 11	245	429.8	66.5
Test 12	245	429.8	66.5
Test 13	246	431.6	66.6
Test 14	247	433.3	66.8
Test 15	245	429.8	66.5
Test 16	221	387.7	63.2
Test 17	207	363.2	61.3
Test 18	213	373.7	62.1
Test 19	224	393.0	63.6
Mean	230.6	404.6	64.5
Variability (95% confidence level)	25.3	44.4	±3.7
Thermocouple measurement data			63.5± 2.32° C (95% confidence)

Table 7. Test results from test 2b
(6 amps to flow heater, 23.3 - 43.3°C IR temperature range).

	Measured Gray Scale	SRF Corrected Gray Scale	SRF Corrected Temperature (°C) (Equation 12)
Test 1	172	301.8	46.9
Test 2	165	289.5	45.9
Test 3	167	293.0	46.2
Test 4	172	301.8	46.9
Test 5	172	301.8	46.9
Test 6	173	303.5	47.0
Test 7	182	319.3	48.2
Test 8	166	291.2	46.0
Test 9	168	294.7	46.3
Test 10	170	298.2	46.6
Test 11	172	301.8	46.9
Test 12	174	305.3	47.2
Test 13	176	308.8	47.4
Test 14	177	310.5	47.6
Test 15	177	310.5	47.6
Test 16	166	291.2	46.0
Test 17	183	321.0	48.4
Test 18	182	319.3	48.3
Mean	173	303.5	47.0
Variability (95% confidence level)	11.0	19.4	±1.6
Thermocouple measurement data			43.7± 1.6°C (95% confidence)

5.5 DISCUSSION

The infrared measured temperatures from Table 2 and Table 5 agree with the temperature measured with the calibrated thermocouple within the combined uncertainty of the IR camera and the thermocouple. The best match attainable was with the emissivity set on the IR camera at 0.88 and 0.95 for each specimen respectively. The emissivity setting is adjustable in increments of 0.01 and the affect on the gray scale output is highly non-linear (Herring [1992]). A slight change in the emissivity was noted to have a large effect on the gray scale (and therefore temperature) output from the infrared imaging system during the emissivity determination portion of the experiment. Measuring the emissivity over a wide variety of temperatures could result in better measurement accuracy for future work.

The SRF correction was critical to obtain accurate results in tests included in Table 3, Table 4, Table 6 and Table 7. The effect of the SRF correction is more visible in test 2 (Tables 6 and 7) due to the smaller target angle (and smaller SRF value). If the gray scale outputs in test 2 would have been utilized directly the results would have been as follows:

Test 2 (part a)

Gray Scale = 230.6

Uncorrected Temperature = 50.9°C

SRF Corrected Gray Scale = 404.6

Corrected Temperature = 64.5°C

Flow Temperature = 63.5°C

Test 2 (part b)

Gray Scale = 173

Uncorrected Temperature = 36.8°C

SRF Corrected Gray Scale = 303.5

Corrected Temperature = 47.0°C

Flow Temperature = 43.7°C

The infrared camera measurements from part a in both tests (Table 3 and Table 6) appear more accurate than the results from part b (Table 4 and Table 7). The infrared measurement results in Table 7 are the least accurate. The confidence regions of the temperature measured by the IR camera and the thermocouple do not overlap in Table 7. This could be the result of increased experimental uncertainty from the lower temperature in test 2b decreasing the ratio of emitted radiation to reflected radiation (signal to noise). The inaccuracy of the SRF prediction in Table 7 may also be compounded by the extrapolation beyond the temperature range setting on the Inframetrics 600L infrared camera. It is also interesting to note that the 95% confidence regions on the thermocouple and the infrared measurements are the smallest in this particular test. It may be that the narrow confidence regions are somewhat of an anomaly and that re-testing would show that the confidence regions would overlap.

A third possibility is a change in the emissivity of the component. Other researchers have noted that the apparent emissivity of semi-conductors can vary over the temperature ranges investigated here (Okamoto and Inagaki [1994], Inagaki et al [1994], Daryabeigi et al. [1992]). Figure 30 presents results from Inakaki et.al [1994].

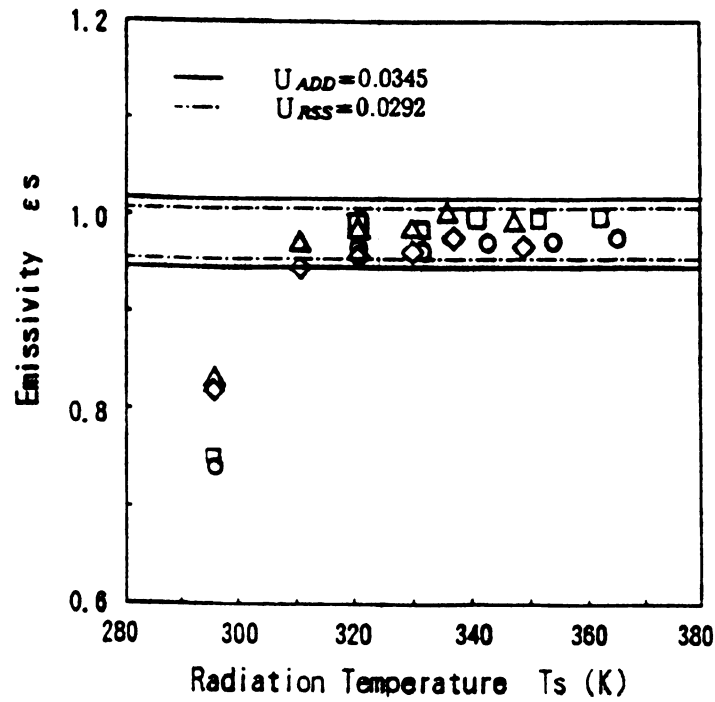


Figure 30. Emissivity variation observed in semi-conducting materials by Inagaki et.al., 1994.

The infrared measured temperature would appear to be insensitive to variance in the emittance if the radiosity - black body temperature relationship,

$$E_b(T) = \frac{J(T, T_\infty, \epsilon) - (1 - \epsilon)E_b T_\infty}{\epsilon}, \quad (18)$$

is considered, where E_b is the equivalent blackbody emission and J is the radiosity measured by the infrared sensor (Welch and Van Gemert [1995]). The radiosity, J , is proportional to the fourth power of absolute temperature (the Stephan-Boltzmann law). The blackbody emission - temperature relationship is also non-linear and for the 8-12 μ m wavelength band maybe curve fit with a fifth order polynomial (Welch and Van Gemert [1995]). The Inframetrics infrared camera utilizes an internal transfer function in the

hardware to manipulate this relationship to obtain temperature and electronically adjusts for the reflected radiation. At elevated target temperatures, the ratio of the emitted radiation to the reflected radiation (from the environment) is larger and thereby reduces error by reducing the signal to noise ratio. A variation in the measured radiosity will be approximately proportional to the fluctuation in the temperature, a variation in the emissivity will affect the temperature result differently at different temperatures with the sensitivity to emissivity variation increasing with the temperature. Valvano and Pearce [1995] state that "...all of the errors in thermal imaging contribute to an under-estimation of the true surface emitted flux, ϵE_b , and thus an underestimate of surface temperature is obtained". A simple analytical model relating the black body emission and the camera radiosity measurement was created. A trend similar to the one presented was noted, the computed IR output was consistently below the "true" temperature and the error was increased at smaller temperature differences between the target and the ambient conditions. This could be corrected by decreasing the emissivity at lower temperatures indicating that the emissivity perceived by the IR camera decreases as the target temperature approaches the ambient condition. However, these results presented could not be replicated exactly.

It is also unclear if this is a change in the actual emissivity or the emissivity as perceived by the infrared camera in specific wavelengths viewed. However, either effect will alter the measurements.

The SRF correction does improve the accuracy of the infrared camera when imaging unresolved targets. The measurement error (Φ) as defined in

$$\Phi = \frac{(T_{SRF} - T_{actual})}{(T_{IR} - T_{actual})} . \quad (19)$$

was reduced by at least 50% (47.8% in Table 7) in the results presented (T_{SRF} is the SRF corrected temperature, T_{IR} was the uncorrected IR temperature measurement). Typically the correction adjusted the infrared measurement so that the actual temperature was included within the measurement uncertainty range of the infrared camera. In the worse case, the thermocouple and IR camera confidence ranges do not overlap by a gap of 0.1°C .

Another method to review the data is to perform a null hypothesis statistical test to determine if the difference between the corrected value and the SRF corrected value is statistically significant. A standard z test statistic (Miller and Freund [1965]) can be defined as

$$z = \frac{(\bar{x}_1 - \bar{x}_2)}{\sqrt{\frac{\sigma_1^2}{n_1} + \frac{\sigma_2^2}{n_2}}} , \quad (20)$$

where z is the test statistic that will be compared to a Student's t statistic to determine the confidence level, \bar{x} is the mean value, σ is the standard deviation and n is the total number of data points. The results of applying the null hypothesis test are shown in Table 8 which also includes a summary of the true values (as measured with a calibrated thermocouple) and the SRF corrected values.

Table 8 indicates that at the higher temperature values the SRF corrected value and the true value are statistically indistinguishable. Test 1b with the MAF sensor almost passed the statistical test (it failed by 0.1 and is marked No***). Test 2b with the cylinder

failed. It is important to note that the uncorrected value for test 2b was further from the true value than the SRF corrected estimate.

Table 8. Null hypothesis statistical test results.

	MAF Sensor $\theta = 0.007$ radians $\varepsilon = 0.88$ SRF Corrected Temperature	SRF = 0.90 True Temperature	Number of Data Points	95% Null Hypothesis
Test 1a	60.9 ± 5.1	61.0 ± 3.4	n = 13	Yes
Test 1b	38.1 ± 3.2	36.6 ± 1.9	n = 14	No***
	Cylinder $\theta = 0.0029$ radians $\varepsilon = 0.95$ SRF Corrected Temperature	SRF = 0.57 True Temperature		
Test 2a	64.5 ± 3.7	63.5 ± 2.3	n = 19	Yes
Test 2b	47.1 ± 1.6	43.7 ± 1.6	n = 18	No

In conclusion, the application of the SRF correction procedure outlined in section 5.2 can reduce thermal measurement errors by at least 50%. This improvement extends the capabilities of the HTRL and the applications of the Inframetrics 600L infrared camera. The error created by imaging unresolved thermal images was substantially reduced. The application of the SRF correction does increase the experimental uncertainty. The uncertainty in the experiments presented above was approximately ± 2.5 °C. This uncertainty can be derived from the variability of the SRF function or from the variability of the particular experiment as shown in Tables 3, 4, 6 and 7 by utilizing Equation 17. It is recommended that the specific experimental variability be applied if possible.

CHAPTER 6. CONCLUSIONS

A facility was constructed to provide air flows of known velocity profiles and temperatures with the necessary sensors to monitor these parameters. The facility was characterized specifically to study small scale devices with the infrared imaging system in the HTRL. A procedure to calibrate the infrared imaging system and the associated data acquisition equipment was developed. The slit response function (SRF) for the infrared system was experimentally measured for the basic system and with the external optics (3x telescopic lens and the 6" close up lens). A procedure to use the SRF to correct experimental measurements was defined along with the increase in the uncertainty in the corrected temperature. Finally, an experimental verification of the procedure was conducted.

The experiments contained in the investigation presented were all conducted under the calibration nozzle with the airflow heater in place. This provided an environment with known and controlled velocity and temperature profiles to compare the infrared radiometer measurements against. The control of these environmental conditions were utilized to simulate "unknown" operating conditions.

A wind tunnel facility was designed to expand the experimental capabilities of the HTRL and to support the current research project. The facility contains a two-dimensional flow contraction that is being characterized currently for a separate project. The facility also has the capability to inject steam into the flow to study the effects of humidity in experiments. The experimental facility contains a traverse system to take detailed spatial measurements and custom software to control the traverse system and acquire data. The details of the system are contained in Chapter 2.

The infrared imaging system and the associated data acquisition system were calibrated to obtain the maximum useful dynamic range. This procedure was outlined in Chapter 3. The result of this calibration was the inclusion of 95% of the dynamic range with a linear response over the entire measurement extent. These results agree very well with the ideal system response that was defined as the goal of the calibration.

The SRF function determined for the Inframetrics 600L infrared camera did not agree with the manufacture's specifications. This was determined to be the result of delinquent calibrations and potentially contaminated lenses in the optical path. The SRF measured was repeatable and appeared to be steady over the time frame of the work presented here. Understanding the SRF is critical to obtaining valid thermal measurements on objects near the limits of the IR camera resolution.

Figure 31 presents the SRF correction factor (CF) and associated uncertainty as a function of target size for the Inframetrics camera with the close up optics. The SRF correction (Figure 31) reduces the amount of error when imaging targets smaller than the thermal measurement resolution. There is an increase in the uncertainty associated with these measurements as the target angle is reduced. The mean temperature correction can be substantial (changing the gray scale value by up to and exceeding a factor of 10) and the uncertainty of this correction can be increased to as much as 25% of the correction for target sizes below 0.25 mm.

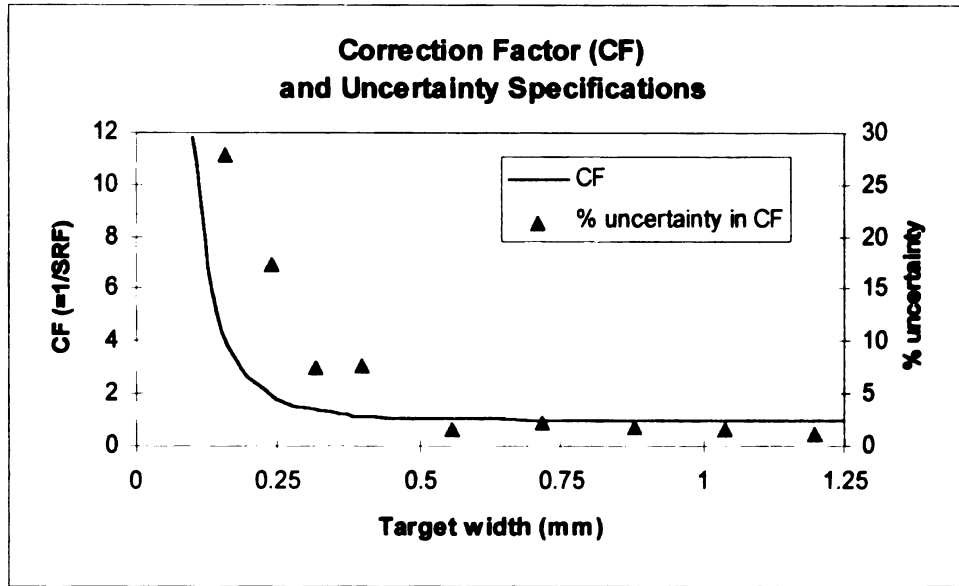


Figure 31. Correction factor (1/SRF) and % uncertainty in CF for Inframetrics 600L IR camera with close up optics in place as a function of target size.

Target emissivity can be measured within each thermal measurement resolution (TMR). The TMR for the Inframetrics camera with the close up optics is 700 μm .

The experimental verification of the SRF correction (Chapter 5) shows that the method provides a valid measurement correction and reduces the error associated with measuring unresolved thermal targets.

The goal of the original research proposal was to apply infrared thermography to the calibration of the MAF sensors. The MAF sensor resistance as a function of temperature can be determined utilizing an ohm-meter and the IR camera. Furthermore, the sensor can be heated electrically in a flow field and its temperature determined with the infrared system. This flow configuration can be utilized with a standard Nusselt correlation (Incorpera and Dewitt [1990]) such as

$$Nu = \frac{hD}{k} = CRe_D^m Pr^{\frac{1}{3}}, \quad (21)$$

with C and m as calibration coefficients, the Reynolds number (Re) defined in Equation 4, the Prandtl number for air (Pr), and the heat transfer coefficient (h) defined as

$$h = \frac{I^2 R}{A(T_{MAF} - T_{flow})}, \quad (22)$$

where $I^2 R$ is the Joule heating occurring and A is the surface area of the sensor. All of these variables can be measured directly and the constants C and m can be obtained from an ordinary least squares curve fit procedure. The variable m is approximately 0.5 which will cause the velocity and the temperature measured by the infrared camera to be related as

$$V \propto \frac{1}{(T_{MAF} - T_{flow})^2}. \quad (23)$$

Equation 23 can be utilized to reduce the error in the velocity calculation created by uncertainty in the MAF sensor temperature by maximizing the $(T_{MAF} - T_{flow})$ quantity. This is advantageous with the results presented here because the SRF correction is more accurate at higher temperatures as discussed previously. These results indicate that the original goal of the project can be obtained.

CHAPTER 7. RECOMMENDATIONS FOR FUTURE WORK

7.1 SLIT RESPONSE FUNCTION

The SRF determined for this camera is not within specifications for the system as manufactured. This could be the result of optical misalignment, optical contamination or possibly scanner calibration. Inframetrics recommends that the 600L infrared camera be re-calibrated each year. The camera used for the experiments has not been re-calibrated for at least 3 years. The multi-point calibration consists of viewing a blackbody at known temperatures and adjusting the electronic processing to the correct value. The scanning optics are also realigned and cleaned during this procedure.

Any combination of these issues can cause the SRF function to degrade. Nevertheless, the results presented here can still be considered valid for the scanner in question because it is repeatable. Studies in the future should measure the SRF function to see if it has drifted further. If the system is re-calibrated or if the optics are cleaned, it is expected that the SRF will improve.

7.2 INFRARED CAMERA RESPONSE TO TEMPERATURE GRADIENTS

The SRF determines the infrared system response to a step function in temperature. Typically a step function will only occur at the edges of the target. An extension of the SRF work would be to quantify the maximum temperature gradient that the infrared detector can accurately measure. This would be especially relevant in experiments involving heat transfer such as steady state conduction with a large heat flux (Q) through a material with a low thermal conductivity (k) as shown in

$$\frac{dT}{dx} = \frac{Q}{k}. \quad (20)$$

Gartenberg and Roberts [1990] conducted a study in which electrically heated wires were suspended in an air flow and imaged with an infrared system. The target was unresolved optically but this was corrected for with the use of an ‘apparent’ emissivity. They found that while the IR imaging system could accurately measure the wire center (where $dT/dx = 0$), as the gradient increased, the measurement accuracy decreased.

7.3 HOT-WIRE SENSORS

Preliminary work was performed with 2 hot wire sensors in the flow field to measure both temperature and velocity simultaneously. Computer code was written to solve the two equations iteratively for the two variables and is included in Appendix 3. It appears that the maximum accuracy and sensitivity to both velocity and temperature can be obtained by setting one over-heat ratio as high as possible (approximately 1.7 for tungsten hot wires) and the other over-heat ratio reasonably low. Preliminary experiments have shown that an overheat value of 1.3 provides heightened sensitivity to the flow temperature.

Five micron diameter platinum wire has been ordered. This wire is more stable in an oxygen environment and can be run at an over-heat of up to 2.2. This wire will be evaluated for future work. It is expected that the larger difference in the over heat values will reduce measurement errors in both temperature and velocity. The platinum wire will also be evaluated as a cold wire sensor. This is very similar to hot wire measurement

methods except that a minimum electrical sensing current is used to measure the resistance of the wire. The resistance is sensitive to temperature changes and therefore will allow the wire to be calibrated and used to measure temperature directly. The cold wire is insensitive to flow velocity and the output can be utilized to temperature compensate the hot-wire output.

7.4 DATA ACQUISITION

Several improvements are scheduled for the data acquisition system. These include obtaining two 200MHz Pentium computer configured as follows:

- A. Pentium 200MHz computer with 32 Mbytes of RAM w/
 - a. A Keithley-MetraByte DAS-TC/b board
 - b. A DAS-1802 333kHz data acquisition board
- B. Pentium 200MHz computer with 32 Mbytes of RAM w/
 - a. Image-Pro Plus v3.0.1 for Windows 95 software
 - b. Data Translations DT3152 Frame Grabber board

The Pentium computer with the DAS-TC and the DAS-1802 board will greatly enhance the data acquisition capabilities and the speed at which data can be obtained. A single DAS-TC board is being used for all thermocouple and hot wire data captures. This board limits the data acquisition rate to 25Hz on each channel. This is much too slow to capture any flow features aside from the mean velocity. At this rate, a data file of 1000 data points from a single hot wire and a single thermocouple requires 40 seconds. This is the equivalent to 20,000 slot widths of flow (10 m/s velocity with an exit width of 2 cm),

essentially, 1 data point every 20 slot widths of flow. This is much too slow to capture transient events. It is also possible that periodic events in the flow (such as vortex shedding) could suffer from measurement aliasing and not be captured or understood from the data obtained.

The DAS-TC/b board will be utilized for thermocouple and humidity sensor measurements. These sensors have relatively slow response times due to the nature or mass of the sensor (the bead size of the thermocouple or the capacitor in the humidity probe). The DAS-1802 board will be used strictly to control the stepper motor motions and to read the data from the hot wires and the pressure transducer. The DAS-1802 with 3 channels active is capable of acquiring data at 100 kHz per channel. This will allow 200 data points per slot width of flow.

The increase in data rate as well as the increase in memory will also help to insure data is convergence. The current system is limited to 2 data channels with 4000 points each. This results in a cumulative average shown in Figure 31. The cumulative average appears to be converged within 4000 data points.

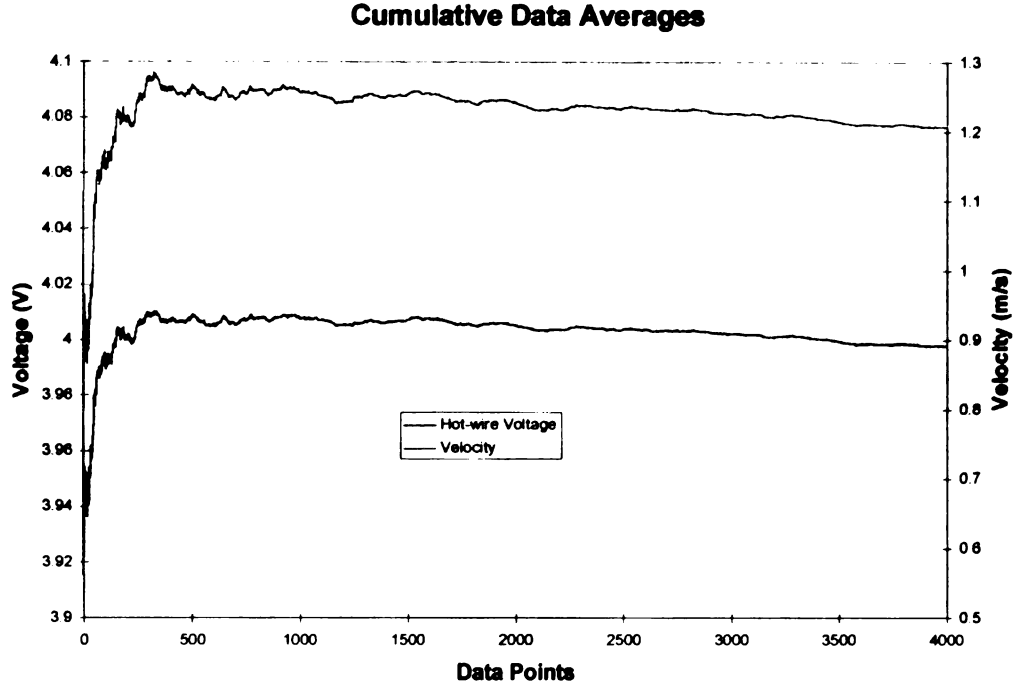


Figure 32. Cumulative average of the hot-wire data.

A method for quantifying the degree of convergence is presented by Mandel [1964] as shown in

$$L = \sqrt{\frac{4t^2 \hat{\sigma}^2}{n}}. \quad (23)$$

This equation uses the Student t statistic (t) and the estimated standard deviation (σ) with the number of degrees of freedom (data points) (n) to estimate the uncertainty (L) in the mean value. The confidence level is obtained from the Student t statistic. The distribution of the data is assumed to be gaussian and n was always greater than 1000 data points.

The data in Figure 31 has a mean velocity of 1.21 m/s with a standard deviation of 0.718 m/s. When Equation 23 is applied to the data utilized in Figure 31, the estimated uncertainty in the mean is 0.045 m/s at a 95% confidence level. If a 99% confidence level

is desired, the uncertainty becomes 0.058 m/s. Typically in this study, 2000 data points were utilized for hot-wire and thermocouple measurements. This results in an uncertainty of 0.063 m/s with a 95% confidence for the hot-wire data shown in Figure 31.

This information also indicates the need for the new data acquisition boards. The equipment utilized for this study acquired data at 25 Hz, thus, it took 40 seconds to obtain 1000 data points. This is much too long for transient flow tests and made steady state tests take much longer than necessary. The longer each experiment was run, the greater the drift in the ambient temperature, the greater the drift in the hot-wire calibration and the greater the chance that a particle would ruin the hot-wire and the entire data set.

APPENDICES

APPENDIX 1. TWO-DIMENSIONAL FLOW CONTRACTION

The design for the two-dimensional contraction was taken from Morrel [1977]. The method designs the contraction by using two cubic functions and matching the slopes so that the flow experiences a favorable pressure gradient to prevent separation along the contraction surfaces and a gradual smooth change in the derivative of the profile shape.

The design process outlined by Morrel is iterative. A program was written in Mathematica[®] to simplify the design process and to plot the resultant profile. The Mathematica[®] program is included at the end of this appendix.

The contraction can be seen in Figure 33 and the manufacturing coordinates are detailed in Table 9. The contraction was manufactured from 1/4" thick Lexan[®] by machining the necessary profile in a suction mold. The Lexan was heated until it became pliable and then was pulled into its final shape by the vacuum applied. The machining and forming was completed by Prodigy Machine and Gage, Lansing Michigan.

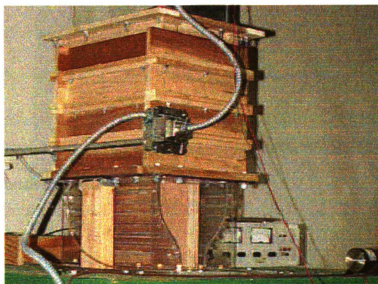


Figure 33. Two-dimensional flow contraction.

Table 9. Two dimensional contraction machining coordinates.

x (meters)	y (meters)		x (meters)	y (meters)
0	0.1905		0.115	0.12951
0.005	0.190495		0.12	0.121203
0.01	0.19046		0.125	0.112175
0.015	0.190365		0.13	0.102395
0.02	0.190179		0.1335	0.095086
0.025	0.189873		0.135	0.091924
0.03	0.189417		0.14	0.082231
0.035	0.188781		0.145	0.07378
0.04	0.187933		0.15	0.066484
0.045	0.186846		0.155	0.060259
0.05	0.185487		0.16	0.05502
0.055	0.183828		0.165	0.050682
0.06	0.181838		0.17	0.047159
0.065	0.179487		0.175	0.044368
0.07	0.176745		0.18	0.042222
0.075	0.173582		0.185	0.040637
0.08	0.169968		0.19	0.039529
0.085	0.165872		0.195	0.038811
0.09	0.161265		0.2	0.038399
0.095	0.156117		0.205	0.038208
0.1	0.150398		0.21	0.038153
0.105	0.144077		0.215	0.038149
0.11	0.137124			

The next two pages contain the Mathematica program written to show the profile and to aid the iterative process.

```
Clear[H1, H2, x, Ha, Hb, EX, L]
```

$$H1 = \frac{.1905}{2};$$

$$H2 = \frac{.03815}{2};$$

```
L = 0.213;
```

```
EX = 0.627;
```

$$Ha[x_] = H2 + (H1 - H2) \left(1 - \frac{\left(\frac{x}{L}\right)^3}{EX^2} \right);$$

$$Hb[x_] = H2 + \frac{(H1 - H2) \left(1 - \frac{x}{L}\right)^3}{(1 - EX)^2};$$

```
Hpa[x_] = D[Ha[x], x];
```

```
Hpb[x_] = D[Hb[x], x];
```

```
Plota = Plot[Ha[x], {x, 0, .1336}, PlotLabel -> "Contraction Profile",
```

```
DisplayFunction -> Identity];
```

```
Plotb = Plot[Hb[x], {x, .1336, 0.213}, DisplayFunction -> Identity];
```

```
Plotc = Plot[Hpa[x], {x, 0, .1336}, DisplayFunction -> Identity];
```

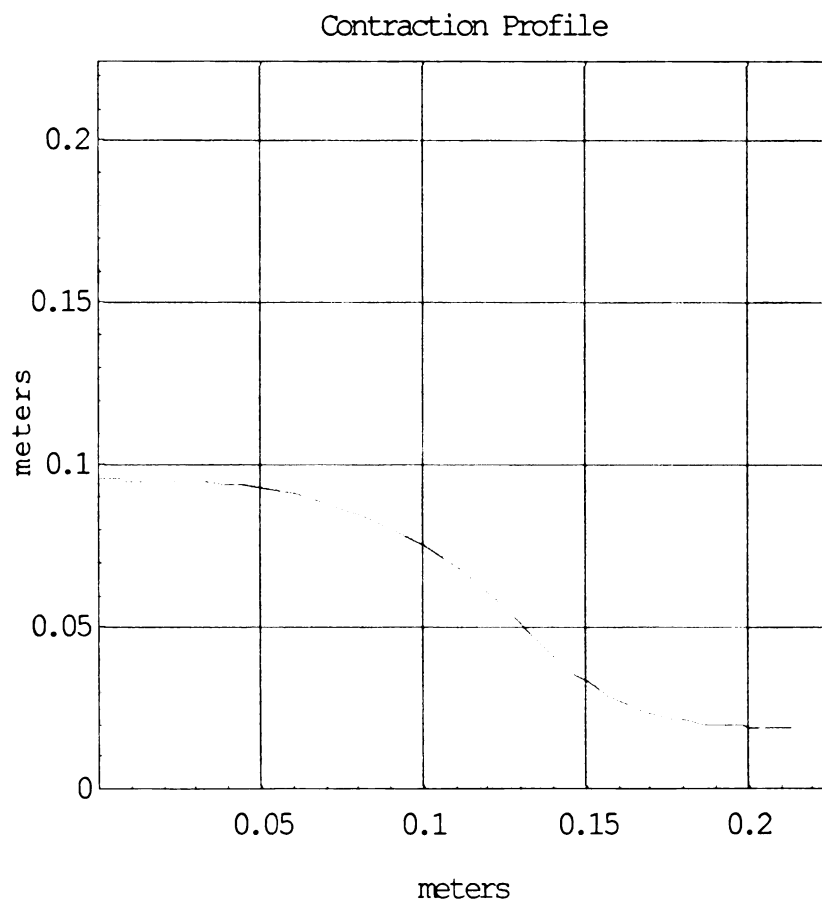
```
Plotd = Plot[Hpb[x], {x, .1336, 0.213}, DisplayFunction -> Identity];
```

```
Show[Plota, Plotb, DisplayFunction -> $DisplayFunction, AxesOrigin -> {0, 0},
```

```
Frame -> True, GridLines -> Automatic, PlotRange -> {{0, .225}, {0, .225}},
```

```
AspectRatio -> 1  $\frac{1}{1}$ , FrameLabel -> {meters, meters}]
```

Output Graphics



APPENDIX 2. QUICKBASIC[®] PROGRAM TO PERFORM DATA ACQUISITION AND STEPPER MOTOR CONTROL

The following is a quick basic program developed and written by Dr. John McGrath and Paul Hoke to operate the data acquisition and stepper motor boards. This program allows for the stepper motor to move to position in increments of $6.602\ \mu\text{m}$ (this is determined by the motor and mechanical translation device). The stepper motor control consists of a CMD-50 chopper drive and a VCO-4050 controller board from American Precision Industries. The stepper motors are controlled from the data acquisition board inputs and outputs. The data acquisition card is a DAS-TC utilized in conjunction with a DAS-02 card from Keithly-MetraByte. These boards collect 16 channels of input and are capable of driving 2 channels of analog output.

REM This is the program recalb.bas

REM WEDNESDAY, Dec 17, 1997: 12:10 PM

' Include the supplied Q4IFACE.BI file. This file

' contains all function DECLARAtion supported by the driver for the DASTC board.

' \$INCLUDE: 'Q4IFACE.BI'

'-----

' Define ALL local variables required by the program here. NOTE

' that you must avoid declaring and using QuickBASIC variables on the

' fly.

DIM NumOfBoards AS INTEGER

DIM DERR AS INTEGER

DIM DEVHANDLE AS LONG

DIM BoardNum AS INTEGER

DIM CJC AS SINGLE

DIM CHAN AS INTEGER

DIM GGAIN AS INTEGER

DIM ADDATA AS LONG

DIM TEMPGBV AS LONG

DIM TEMPGB AS SINGLE

DIM TEMPINV AS LONG
DIM TEMPIN AS SINGLE
DIM TEMPOUTV AS LONG
DIM TEMPOUT AS SINGLE
DIM TEMPSURFV AS LONG
DIM TEMPSURF AS SINGLE
DIM RELHUMV AS LONG
DIM RELHUM AS SINGLE
DIM PDIFFV1 AS LONG
DIM PDIFFV AS SINGLE
DIM HWV11 AS LONG
DIM HWV1 AS SINGLE
DIM HWV21 AS LONG
DIM HWV2 AS SINGLE
DIM dp1 AS LONG
DIM dp AS SINGLE
DIM tc1 AS LONG
DIM J AS LONG
DIM NUMBER AS LONG
DIM SUM1 AS SINGLE
DIM SUM2 AS SINGLE
DIM SUM3 AS SINGLE

```

DIM SUM4 AS SINGLE

DIM HW1AVEL AS SINGLE

DIM HW2AVEL AS SINGLE

DIM dpavg AS SINGLE

DIM HWV1(2000)

DIM HWV2(2000)

DIM dp(2000)

DIM tcf(2000)

DIM VINVISCID AS SINGLE

DIM DELP AS SINGLE

'OPEN FILES FOR WRITING HOTWIRE DATA

'OPEN "HW1.DAT" FOR OUTPUT AS #1

'OPEN "HW2.DAT" FOR OUTPUT AS #2

'OPEN "dp.dat" for OUTPUT as #3

CLS

'-----

' This step initializes the internal data tables according to the

' information contained in the configuration file DASTC.CFG.

PRINT "Initializing the DASTC board - - - PLEASE wait"

a$ = "DASTC.CFG" + CHR$(0)

DERR = DASTCDEVOPEN%(SSEGADD(a$), NumOfBoards)

IF DERR <> 0 THEN

```

```

BEEP

PRINT "ERROR "; HEX$(DERR); " OCCURRED DURING '..DEVOPEN'"

STOP

END IF

BoardNum = 0

DERR = DASTCGETDEVHANDLE%(BoardNum, DEVHANDLE)

IF (DERR <> 0) THEN BEEP: PRINT "ERROR, DEVICE HANDLE IS null. . .":

STOP

CLS

REM This part of the program is using the DAC-02 board to control sensor motion

REM Set base address at 784 for DAC-02 board to NOT conflict w/ DAS-TC board

BaseAddr% = 784

REM D/A Output Channels are defined

REM Channel#0 will be used for MOTION: move (>2.5 v; OutData% = 4095)

REM or stop (<2.5 v; OutData% = 0 )

REM Channel#1 will be used for DIRECTION: up/down or in/out for vertical and lead
screw assemblies

REM Set initial voltages on D/A channels to 0. This Means that Channel0 volts = 0 ->
motor stopped

REM Output 0 volts on Channel#1 (DIRECTION); Ch$1 first because of prob detected

Ch1% = 1

OutData% = 0

```

```

HByte% = INT(OutData% / 16)          'Convert to high byte

LByte% = 16 * (OutData% - HByte% * 16)  'Convert to low byte

lowport1 = BaseAddr% + 2 * Ch1%

OUT lowport, LByte%          'Write low byte

hiport1 = BaseAddr% + 2 * Ch1% + 1

OUT hiport1, HByte%          'Write high byte

REM Output 0 volts on Channel#0 (MOTION)

Ch1% = 0

OutData% = 0

HByte% = INT(OutData% / 16)          'Convert to high byte

LByte% = 16 * (OutData% - HByte% * 16)  'Convert to low byte

lowport0 = BaseAddr% + 2 * Ch1%

OUT lowport0, LByte%          'Write low byte

hiport0 = BaseAddr% + 2 * Ch1% + 1

OUT hiport0, HByte%          'Write high byte

'This segment inputs parameters needed for calculating velocity and local
' temperature in the boundary layer

'Clear screen

CLS

' REQUEST AN INITIAL POSTION DEFINITION FROM USER IN CASE
DIFERENT THAN ZERO

LOCATE 1, 3: INPUT "Define the initial location in the boundary layer (mm): ",
position

```

THE-BEGIN:

'REM Set initial position equal to zero

'position = 0

REM Set initial count equal to zero

count = 0

DIRECTION:

REM Decide which direction to move the motor and use Channel#1 to effect decision

REM Set channel number to zero

LOCATE 2, 3: PRINT "Positive direction (+y) is AWAY from the wall"

LOCATE 3, 3: INPUT "(D/A Ch1) To move HOTWWIRE: TO WALL- Enter 5; AWAY
FROM WALL- Enter 0 ", decide%

IF decide% < 2.5 GOTO OUTDOWN

' LET SIGN = -1 FOR MOTION TO THE WALL

SIGN = -1

REM Output 5 volts on Channel#1 to move IN or UP

Ch1% = 1

OutData% = 4095

HByte% = INT(OutData% / 16) 'Convert to high byte

LByte% = 16 * (OutData% - HByte% * 16) 'Convert to low byte

OUT BaseAddr% + 2 * Ch1%, LByte% 'Write low byte

OUT BaseAddr% + 2 * Ch1% + 1, HByte% 'Write high byte

GOTO END.DIRECTION

OUTDOWN:

REM Output 0 volts on Channel#1 to move OUT or DOWN

' LET SIGN = +1 FOR MOTION AWAY FROM THE WALL

SIGN = 1

Chl% = 1

OutData% = 0

HByte% = INT(OutData% / 16) 'Convert to high byte

LByte% = 16 * (OutData% - HByte% * 16) 'Convert to low byte

OUT BaseAddr% + 2 * Chl%, LByte% 'Write low byte

OUT BaseAddr% + 2 * Chl% + 1, HByte% 'Write high byte

END.DIRECTION:

REM Define distance(s) to be moved (This will require motor-specific calibrations later)

LOCATE 4, 3: INPUT "How far (in mm) should the motor move? ", DISTANCE

count.desired = DISTANCE * 151.352

REM Decide whether or not to move the motor and use Channel#0 to effect decision

REM Set channel number to zero

LOCATE 5, 3: INPUT "Do you wish to move the motor (D/A Ch 0)? (5= move; 0 =
stop) "; decide%

IF decide% < 2.5 GOTO DONTMOVE

MOVE:

REM output 5 volts on Channel#0 to move motor

Chl% = 0

```

OutData% = 4095

HByte% = INT(OutData% / 16)          'Convert to high byte
LByte% = 16 * (OutData% - HByte% * 16)  'Convert to low byte
OUT BaseAddr% + 2 * Chl%, LByte%      'Write low byte
OUT BaseAddr% + 2 * Chl% + 1, HByte%   'Write high byte

GOTO PULSECOUNT

DONTMOVE:

REM Output 0 volts on Channel#0 to stop motor

Chl% = 0

OutData% = 0

HByte% = INT(OutData% / 16)          'Convert to high byte
LByte% = 16 * (OutData% - HByte% * 16)  'Convert to low byte
OUT BaseAddr% + 2 * Chl%, LByte%      'Write low byte
OUT BaseAddr% + 2 * Chl% + 1, HByte%   'Write high byte

GOTO INFOOUT

PULSECOUNT:

REM This part of the program counts pulses from an A/D channel

REM The DAC-02 board can not be used for this, so the DASTC board will be used.

REM Use Channel#8 for pulse counting

REPEAT:

'get an initial voltage for edge detection in a loop

'The next step gets an initial voltage reading on the pulse counting channel

```


CHAN = 8

GGAIN = 1

,

DERR = KADRead%(DEVHANDLE, CHAN, GGAIN, ADDATA)

IF DERR <> 0 THEN

BEEP

PRINT "ERROR "; HEX\$(DERR); " OCCURRED DURING 'KADRead'"

STOP

END IF

' Calculate the effective voltage.

CALCULATE.VOLTAGE1:

'The next step calculates a voltage from the ADDATA value measured

'Call this first voltage V1

V1 = ADDATA / (1000000)

CHECK:

'this is the beginning of a loop which checks whether successive voltages are different

(>2.5 v) than initial 'voltage

DERR = KADRead%(DEVHANDLE, CHAN, GGAIN, ADDATA)

IF DERR <> 0 THEN

BEEP

PRINT "ERROR "; HEX\$(DERR); " OCCURRED DURING 'KADRead'"

STOP

```

END IF

' Calculate the effective voltage.

CALCULATE.VOLTAGE2:

'The next step calculates a voltage from the second ADDATA value measured

'Call this first voltage V2

V2 = ADDATA / (1000000)

'Calculate the difference between the an initial voltage and all successive voltages in loop

DIFF = ABS(V1 - V2)

'If a 0 to 5 volt or a 5 to 0 volt change is not detected on channel 8, then continue to take
measurements,

'Other wise increment a counter because an edge has been detected.

IF DIFF < 2.5 GOTO CHECK

count = count + 1

IF count > count.desired GOTO the.end

GOTO REPEAT

the.end:

'This stops the motor

Chl% = 0

REM Output 0 volts on Channel#0 to stop motor

OutData% = 0

HByte% = INT(OutData% / 16)           'Convert to high byte

LByte% = 16 * (OutData% - HByte% * 16) 'Convert to low byte

```

```

OUT BaseAddr% + 2 * Chl%, LByte%      'Write low byte
OUT BaseAddr% + 2 * Chl% + 1, HByte%   'Write high byte

' CLEAR SCREEN BEFORE WRITING MOTION INFORMATION TO THE SCREEN
INFOOUT:

CLS

calibration = count / 151.352

position = position + SIGN * calibration

LOCATE 10, 3: PRINT "Hotwire has moved "; calibration * SIGN; "mm"

LOCATE 11, 3: PRINT "Hotwire is now at "; position; "mm"

LOCATE 12, 3: PRINT "Where +x is away from the wall"

DUMMY = 0

LOCATE 15, 3: PRINT "Move again OR set zero position?"

LOCATE 16, 3: INPUT " -1 to quit; 1 to set current position; 0 to move again; 2 TO

TAKE DATA: ", DUMMY

IF DUMMY = -1 GOTO FINISH

IF DUMMY = 1 GOTO ZERO

IF DUMMY = 2 GOTO DATALOOP

GOTO THE.BEGIN:

ZERO:

POSITION = 0

count = 0

GOTO THE.END

```

FINISH:

END

CLS

'WRITE TO SCREEN THE CHOICES MADE FOR DIRECTION AND MOTION

'LOCATE 1, 1: PRINT "YOU CHOSE TO MOVE (UP/DOWN, ETC)"

'LOCATE 2, 1: PRINT "YOUR STARTING STREAMWISE POSITION (X/W) WAS:"

'LOCATE 3, 1: PRINT "YOUR STARTING BOUNDARY LAYER POSITION (Y IN
MM) WAS:"

'LOCATE 4, 1: PRINT "INITIATE LOOPING TO UPDATE EXPERIMENTAL
DATA"

DATALOOP:

CLS

LOCATE 1, 3: PRINT "The Hotwire is now at y= "; position; "mm"

LOCATE 2, 3: PRINT "Where +y is away from the wall"

LOCATE 3, 3: PRINT "The Hotwire is now at x= "; position; "mm"

LOCATE 4, 3: PRINT "Where +x is DOWN- in the Flow Direction"

LOCATE 6, 3: PRINT "Current data are being displayed for checking"

DO

CHECK\$ = INKEY\$

'This section is for measuring experimental variables

'Measure ambient CJC temperature

BoardNum = 0

```

DERR = DASTCGETCJC%(BoardNum, CJC)

IF (DERR <> 0) THEN BEEP: PRINT "ERROR GETTING CJC TEMPERATURE...":
STOP

LOCATE 8, 5: PRINT USING "AMBIENT CJC TEMP(C)= ###.##"; CJC

'Measure TEMPERATURE IN GIELDA BOX, TEMPGB

CHAN = 7

GGAIN = 1

DERR = KADRead%(DEVHANDLE, CHAN, GGAIN, TEMPGBV)

  IF DERR <> 0 THEN

    BEEP

    PRINT "ERROR "; HEX$(DERR); " OCCURRED DURING 'KADRead'"

    STOP

  END IF

TEMPGB = ((TEMPGBV / 1000000) - 1) * 25

LOCATE 9, 5: PRINT USING "TEMPERATURE IN GIELDA BOX (C) = ###.##";
TEMPGB

'Measure PLATE INLET TEMPERATURE, TEMPIN

CHAN = 5

GGAIN = 1

DERR = KADRead%(DEVHANDLE, CHAN, GGAIN, TEMPINV)

  IF DERR <> 0 THEN

    BEEP

```

```

PRINT "ERROR "; HEX$(DERR); " OCCURRED DURING 'KADRead'"

STOP

END IF

TEMPIN = TEMPINV / 100

LOCATE 10, 5: PRINT USING "PLATE INLET TEMPERATURE (C)= ###.##";

TEMPIN

'Measure PLATE OUTLET TEMPERATURE, TEMPOUT

CHAN = 6

GGAIN = 1

DERR = KADRead%(DEVHANDLE, CHAN, GGAIN, TEMPOUTV)

IF DERR <> 0 THEN

    BEEP

    PRINT "ERROR "; HEX$(DERR); " OCCURRED DURING 'KADRead'"

    STOP

END IF

TEMPOUT = TEMPOUTV / 100

LOCATE 11, 5: PRINT USING "PLATE OUTLET TEMPERATURE (C)= ###.##";

TEMPOUT

'Measure PLATE SURFACE TEMPERATURE, TEMPSURF

CHAN = 2

GGAIN = 1

DERR = KADRead%(DEVHANDLE, CHAN, GGAIN, TEMPSURFV)

```

```

IF DERR <> 0 THEN

    BEEP

    PRINT "ERROR "; HEX$(DERR); " OCCURRED DURING 'KADRead'"

    STOP

END IF

TEMPSURF = TEMPSURFV / 100

LOCATE 12, 5: PRINT USING "PLATE SURFACE TEMPERATURE (C)= ###.##";
TEMPSURF

'Measure ambient relative humidity

CHAN = 9

GGAIN = 1

DERR = KADRead%(DEVHANDLE, CHAN, GGAIN, RELHUMV)

IF DERR <> 0 THEN

    BEEP

    PRINT "ERROR "; HEX$(DERR); " OCCURRED DURING 'KADRead'"

    STOP

END IF

RELHUM = ((RELHUMV / 1000000) - 1) / .04

LOCATE 13, 5: PRINT USING "RELATIVE HUMIDITY (%)= ###.##"; RELHUM

'Measure Pressure DIFFERENCE, PDIFF

CHAN = 12

GGAIN = 1

```

```

DERR = KADRead%(DEVHANDLE, CHAN, GGAIN, PDIFFV1)

IF DERR <> 0 THEN

    BEEP

    PRINT "ERROR "; HEX$(DERR); " OCCURRED DURING 'KADRead'"

    STOP

END IF

PDIFFV = PDIFFV1 / 1000000

LOCATE 14, 5: PRINT USING "PRESSURE TRANSDUCER VOLTAGE (VOLTS)=
###.##"; PDIFFV

DELP = PDIFFV * .1

'CHECK FOR NEGATIVE VOLTAGES

IF DELP > 0 GOTO OKSTATE

DELP = 0

OKSTATE:

VINVISCID = SQR((2 / 1.204) * (DELP) * (248.84))

LOCATE 15, 5: PRINT USING "IMPLIES MAX INVISCID JET EXIT PLANE
VELOCITY (m/s)= ###.## "; VINVISCID

'MEASURE CHANNEL 1 HOTWIRE VOLTAGE, HWV1

CHAN = 11

GGAIN = 1

DERR = KADRead%(DEVHANDLE, CHAN, GGAIN, HWV11)

IF DERR <> 0 THEN

```



```

BEEP

PRINT "ERROR "; HEX$(DERR); " OCCURRED DURING 'KADRead'"

STOP

END IF

HWV1 = HWV11 / 1000000

E1 = HWV1

LOCATE 16, 5: PRINT USING "CHANNEL 1 HOTWIRE VOLTAGE (VOLTS)=
###.##"; HWV1

'MEASURE CHANNEL 2 HOTWIRE VOLTAGE, HWV2

CHAN = 10

GGAIN = 1

DERR = KADRead%(DEVHANDLE, CHAN, GGAIN, HWV21)

IF DERR <> 0 THEN

    BEEP

    PRINT "ERROR "; HEX$(DERR); " OCCURRED DURING 'KADRead'"

    STOP

END IF

HWV2 = HWV21 / 1000000

E2 = HWV2

LOCATE 17, 5: PRINT USING "CHANNEL 2 HOTWIRE VOLTAGE (VOLTS)=
###.##"; HWV2;

LOCATE 18, 3: PRINT "PRESS ANY KEY TO INITIATE HOTWIRE DATA
ACQUISITION"

```

GOTO KEYCHECK

KEYCHECK:

LOOP WHILE CHECK\$ = INKEY\$ 'CHECK FOR KEYSTROKE

OOPS:

LOCATE 20, 5: INPUT "ENTER THE NUMBER OF VELOCITY SAMPLES TO BE
TAKEN"; NUMBER

IF NUMBER < 2 GOTO OOPS

'READ HOTWIRE VOLTAGES

'INITIALIZE SUMS TO ZERO FOR AVERAGES

SUM1 = 0

SUM2 = 0

SUM3 = 0

SUM4 = 0

HWV1(0) = 0

HWV2(0) = 0

dp(0) = 0

tcfl(0) = 0

FOR J = 1 TO NUMBER

'MEASURE CHANNEL 1 HOTWIRE VOLTAGE ARRAY, HWVA1(J)

CHAN = 11

GGAIN = 1

DERR = KADRead%(DEVHANDLE, CHAN, GGAIN, HWV11)

```

IF DERR <> 0 THEN

    BEEP

    PRINT "ERROR "; HEX$(DERR); " OCCURRED DURING 'KADRead'"

    STOP

END IF

HWV1(J) = HWV11 / 1000000

SUM1 = SUM1 + HWV1(J)

'MEASURE CHANNEL 2 HOTWIRE VOLTAGE, HWV2

CHAN = 10

GGAIN = 1

DERR = KADRead%(DEVHANDLE, CHAN, GGAIN, HWV21)

IF DERR <> 0 THEN

    BEEP

    PRINT "ERROR "; HEX$(DERR); " OCCURRED DURING 'KADRead'"

    STOP

END IF

HWV2(J) = HWV21 / 1000000

SUM2 = SUM2 + HWV2(J)

'MEASURE CHANNEL 2 HOTWIRE VOLTAGE, HWV2

CHAN = 12

GGAIN = 1

DERR = KADRead%(DEVHANDLE, CHAN, GGAIN, dp1)

```

```

IF DERR <> 0 THEN

    BEEP

    PRINT "ERROR "; HEX$(DERR); " OCCURRED DURING 'KADRead'"

    STOP

END IF

dp(J) = dp1 / 1000000

SUM3 = SUM3 + dp(J)

CHAN = 6

GGAIN = 1

DERR = KADRead%(DEVHANDLE, CHAN, GGAIN, tc1)

IF DERR <> 0 THEN

    BEEP

    PRINT "ERROR "; HEX$(DERR); " OCCURRED DURING 'KADRead'"

    STOP

END IF

tcfl(J) = tc1 / 100

SUM4 = SUM4 + tcfl(J)

NEXT

'CALCULATE THE AVERAGES

HW1AVEL = SUM1 / NUMBER

HW2AVEL = SUM2 / NUMBER

dpavg = SUM3 / NUMBER

```

h2o = dpavg * .1

tcavg = SUM4 / NUMBER

'CALCULATE THE STANDARD DEVIATIONS

hw1st = 0

hw2st = 0

dpst = 0

tcst = 0

FOR J = 1 TO NUMBER

hw1st = hw1st + ((HW1AVAL - HWV1(J)) ^ 2) ^ (.5)

hw2st = hw2st + ((HW2AVAL - HWV2(J)) ^ 2) ^ (.5)

dpst = dpst + ((dpavg - dp(J)) ^ 2) ^ (.5)

tcst = tcst + ((tcavg - tcfl(J)) ^ 2) ^ (.5)

NEXT

hw1stdev = hw1st / (NUMBER - 1)

hw2stdev = hw2st / (NUMBER - 1)

dpstdev = dpst * .1 / (NUMBER - 1)

tcstdev = tcst / (NUMBER - 1)

CLS

LOCATE 11, 5: PRINT USING "CHANNEL 1 HOTWIRE AVERAGE VOLTAGE

(VOLTS)= ##.###"; HW1AVAL

LOCATE 12, 5: PRINT USING "ST.DEV of Hot Wire1 reading (VOLTS) = #.###";

hw1stdev

```

LOCATE 13, 5: PRINT USING "CHANNEL 2 HOTWIRE AVERAGE VOLTAGE
(VOLTS)= ##.###"; HW2AVEL
LOCATE 14, 5: PRINT USING "ST.DEV of Hot Wire2 reading (VOLTS) = ##.###";
hw2stdev
LOCATE 15, 5: PRINT USING "Pressure difference (in/H2O)= ##.###"; h2o
LOCATE 16, 5: PRINT USING "ST.DEV of Pressure reading (in/H2O) = ##.###";
dpstdev
LOCATE 17, 5: PRINT USING "Temperature of Flow = ##.#"; tcavg
LOCATE 18, 5: PRINT USING "ST.DEV of Temperature = ##.###"; tcstdev
'WRITE THE DATA ARRAYS TO TWO FILES: HW1.DAT AND HW2.DAT
'FOR J = 1 TO NUMBER
'WRITE #1, J, HWV1(J)
'WRITE #2, J, HWV2(J)
'WRITE #3, J, dp(J)
'NEXT
'CLOSE THE DATA FILES
'CLOSE #1
'CLOSE #2
'CLOSE #3
LOCATE 24, 3: PRINT "Take another calibration point?"
LOCATE 25, 3: INPUT " -1 to quit; 1 to set current position; 0 to move again; 2 TO
TAKE DATA: ", DUMMY

```

CLS

IF DUMMY = -1 GOTO FINISH

IF DUMMY = 1 GOTO ZERO

IF DUMMY = 2 GOTO DATALOOP

GOTO THE.BEGIN:

APPENDIX 3. FLAT PLATE ISOTHERMAL VELOCITY PROFILES

The velocity profiles taken of the flow below the two dimensional contraction are presented here for completeness. The profiles are not non-dimensionalized in the common format of the velocity divided by the inviscid velocity because at the time of the experiments, there was no pressure tap in the contraction (this has been added since).

These results show the resolution of the stepper motor system combined with the hot wire probes. They also show the flow development below the contraction in a limited fashion. Figure 34 shows all of the data obtained. Figure 35, Figure 36, and Figure 37 show the velocity profiles at each specific X/W location.

The affect of the number of data points can be seen in Figure 34, Figure 36 and Figure 37. The profiles taken with only 200 data points tend to appear jagged, an indication that the measurements at each point were not converged. The profiles with 2000 data points tend to appear smoother and also appear to define a mean value curve among the scatter shown in the 200 data point curves.

The profiles at $x/w = 1.59$ show the inviscid core region of the wall jet as the flat region where $V/V_{max} = 1$. The outer sheared layer and the inner boundary layer progress toward the center of the wall jet as the flow advances in the streamwise (x) direction. This can be seen as the slope becomes more less steep in the outer region and as the flat inviscid central core region disappears.

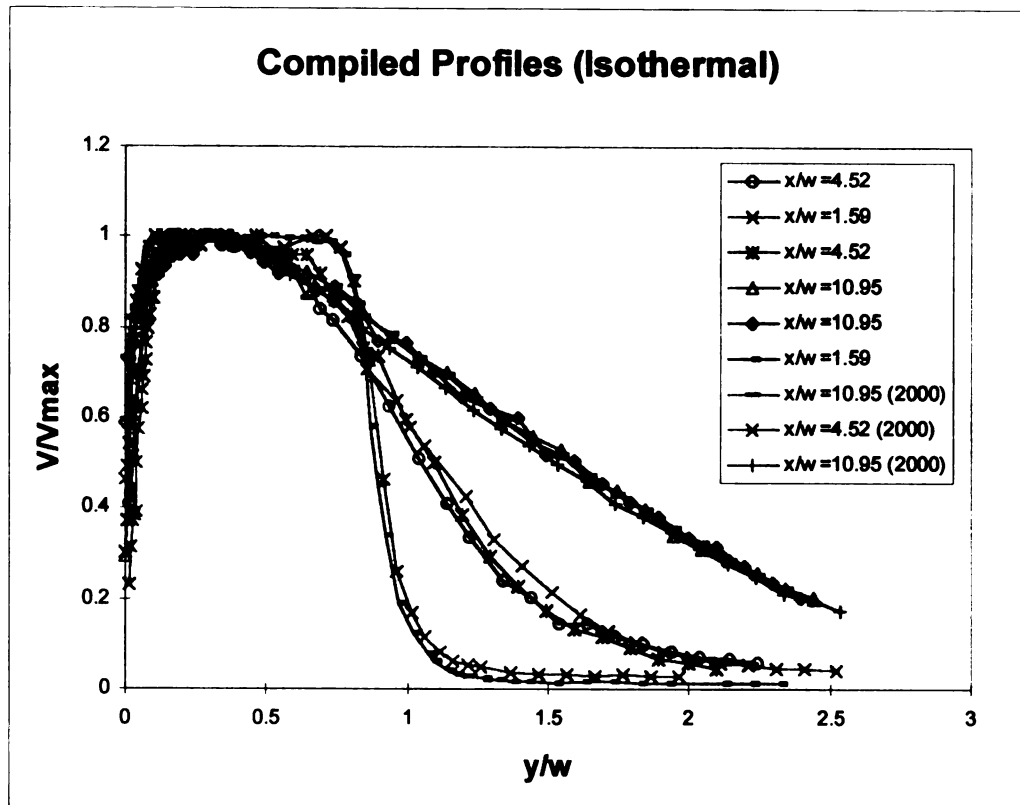


Figure 34. Compiled jet velocity profiles ($w=2$ cm).

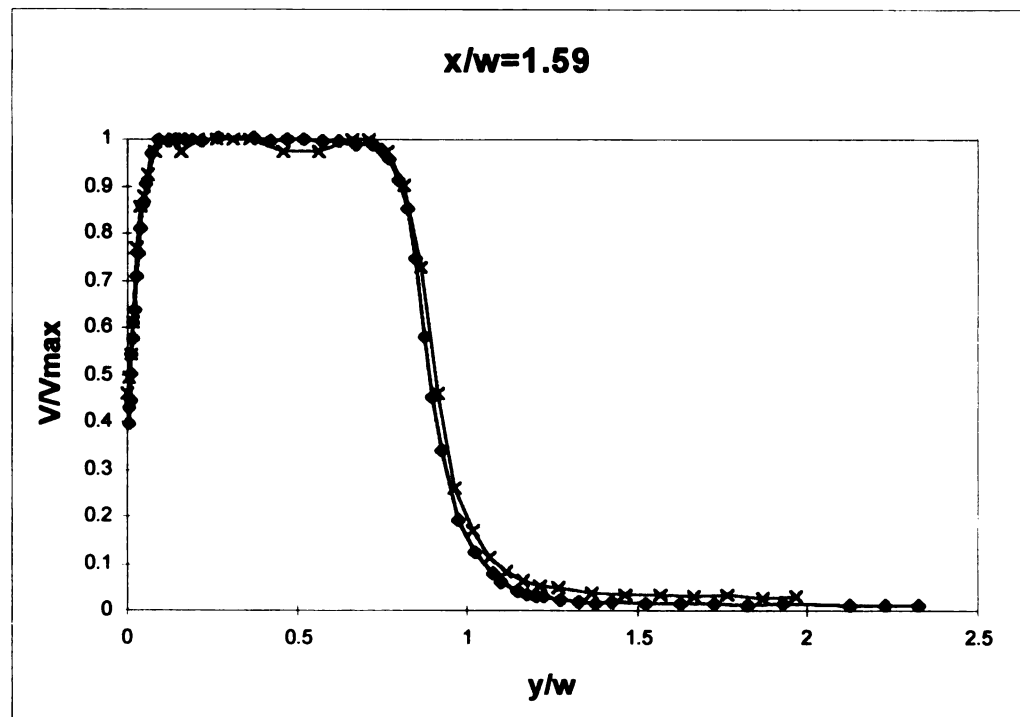


Figure 35. $X/W = 1.59$ velocity profiles ($w=2$ cm).

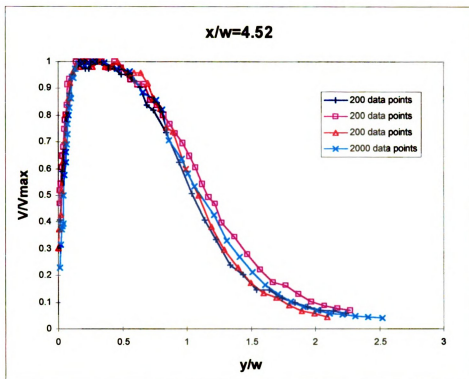


Figure 36. $X/W = 4.52$ velocity profiles ($w=2$ cm).

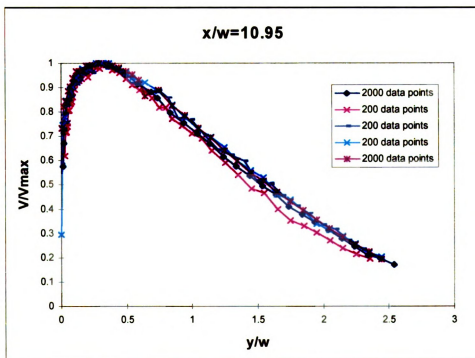


Figure 37. $X/W = 10.95$ velocity profiles ($w=2$ cm).

APPENDIX 4. HOT-WIRE CONSTRUCTION AND CALIBRATION

The hot-wires used in this study were constructed of 5 micron diameter tungsten wire and are schematically shown in Figure 38. The hot-wires were fabricated in the Turbulent Shear Fluids Laboratory (TSFL) at Michigan State University.

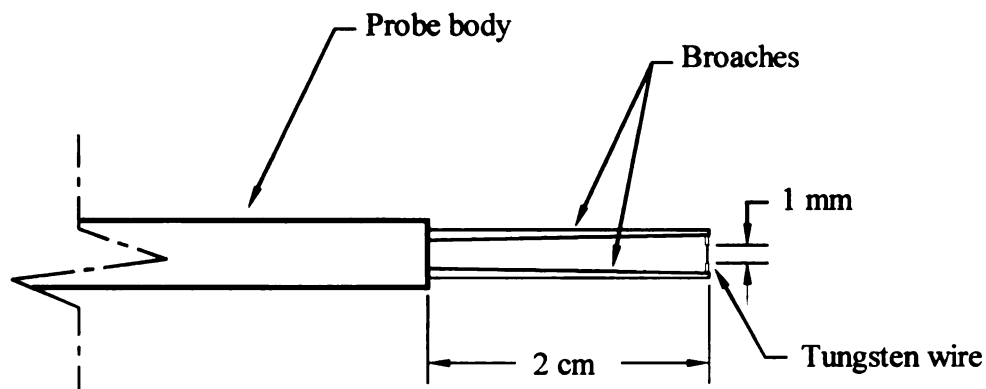


Figure 38. Schematic of hot-wire probe.

The construction procedure, while simple in theory, was very difficult to implement due to the small size of the tungsten wire. The construction procedure is outlined below.

1. The broaches were soaked in flux for 30 seconds. The broaches were dipped slowly into and out of a solder pot to provide a uniform layer of solder.
2. The flux was cleaned off using a flux remover in an ultrasonic bath.
3. A 5 micron tungsten wire was strung across a steel “C” bracket and held in position by adhesive tape.
4. The span was placed in a device so it could be lowered into a copper oxide solution holder to be coated. The span was positioned so that the two regions to be plated were separated by approximately 1 mm (Figure 39).

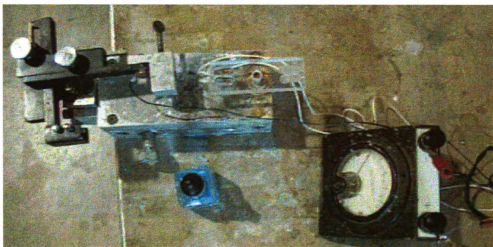


Figure 39. Tungsten wire copper plating station.

6. Power was applied so that approximately 0.8 mA flowed through the device for 8 minutes.
7. The tungsten wire was then soldered across the broaches (Figure 38) using the special solder station to align them properly (Figure 40).

Step seven is by far the most difficult and time consuming. A typical first attempt at manufacturing a hot-wire might take 3 hours. A high level of manual dexterity and practice are required to produce hot-wires with any speed. It is suggested that the entire process could be greatly simplified if the need for human control of the soldering process was eliminated.

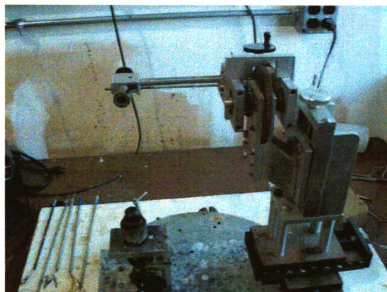


Figure 40. Precision solder station.

Hot-wire calibration requires a well-characterized flow with a known velocity distribution to establish the relationship between the hot-wire output voltage and velocity. A hot-wire calibration system (Figure 41) from the Turbulent Shear Fluids Laboratory (TSFL) was utilized to obtain the first calibration data. This hot-wire calibrator was designed to produce a uniform flow of known velocity (measured with a pressure transducer) with very low turbulence intensity.

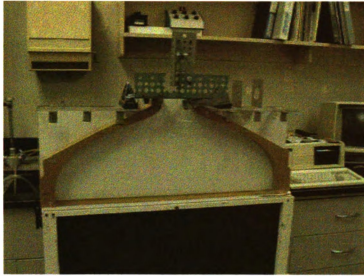


Figure 41. TSFL hot-wire calibration flow contraction.

The hot-wire was taken to the HTRL Flow Facility and mounted beneath the “coke bottle” contraction (Figure 42). This contraction has been well characterized in the TSFL to have a discharge coefficient (C_d) of 0.98 to 1. Assuming that the fluid is incompressible and inviscid, the velocity along a streamline can be calculated from (Blevins [1984])

$$\vec{V} = \sqrt{\frac{1}{1 - \left(\frac{A_2}{A_1}\right)^2}} \times \sqrt{\frac{2(P_1 - P_2)}{\rho}}. \quad (22)$$

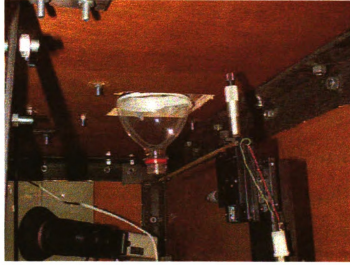


Figure 42. “Coke Bottle” contraction utilized for hot-wire calibration.

Calculating the $(1-(A_2/A_1)^2)^{-1}$ term utilizing the venturi dimensions results in a value of 1.00196. Therefore, it incorporates little error to simplify Equation 22 to

$$\vec{V} = \sqrt{2 \left(\frac{P_1 - P_2}{\rho} \right)}, \quad (23)$$

which is the Bernoulli equation. Furthermore, if area A_1 is considered to be a large hemisphere (control surface) above the nozzle, V_1^2 quickly approaches zero.

A pressure transducer was utilized to measure the difference in static pressure across the contraction, thus allowing the exit velocity to be calculated by applying Equation 23. The density of air was calculated from the ideal gas law.

A typical hot-wire calibration performed in the TSFL contraction resulted in the calibration curve shown in Figure 43. The same hot-wire was then taken to the HTRL Flow facility and calibrated using the same pressure transducer. This resulted in a

calibration curve as shown in Figure 44. The data were curve-fit using TableCurve2D v3 software (AISN [1994]) and the relationship

$$E = \sqrt{A + BV^n} . \quad (24)$$

The coefficients and correlation factors were then used to compare the HTRL facility calibration curves and the calibrations obtained in the TSFL contraction. Typical calibration curves for the TSFL calibrator and the HTRL facility are shown in Figure 43 and Figure 44 respectively. There was less than a 1% difference between the TSFL calibration coefficients and the HTRL facility coefficients. The conclusion was drawn that the HTRL facility could be used for future hot-wire calibration. A pitot tube was later used to verify that the flow velocity below the calibration nozzle agreed with the Bernoulli calculation.

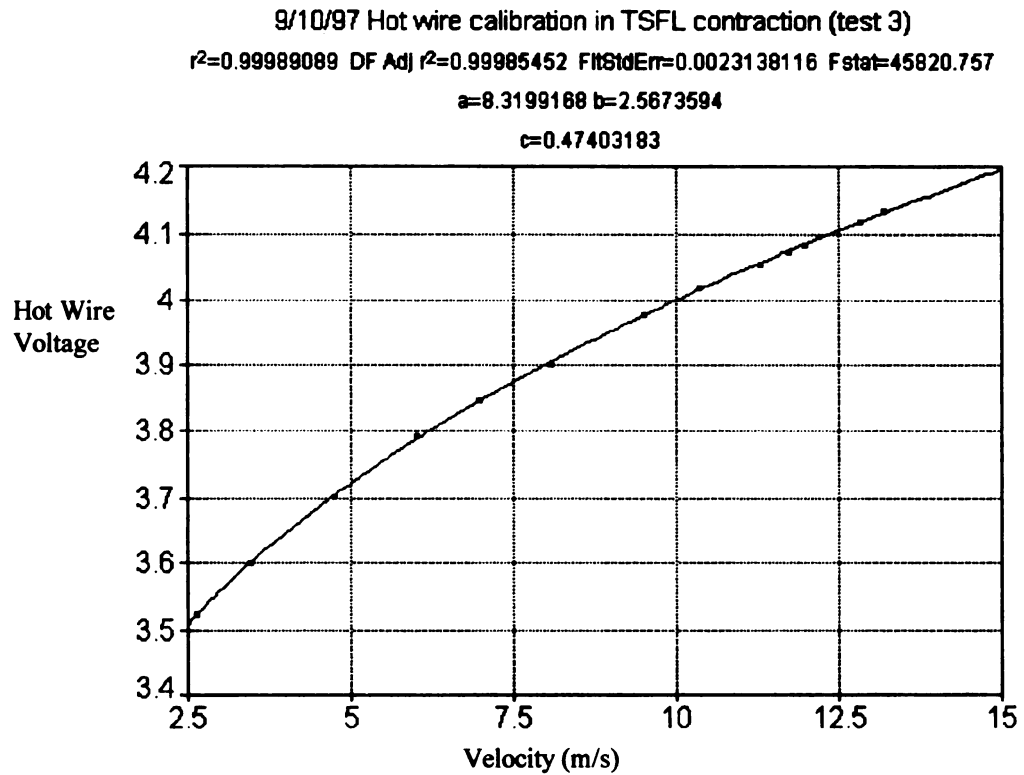


Figure 43. TSFL contraction hot-wire calibration curve.

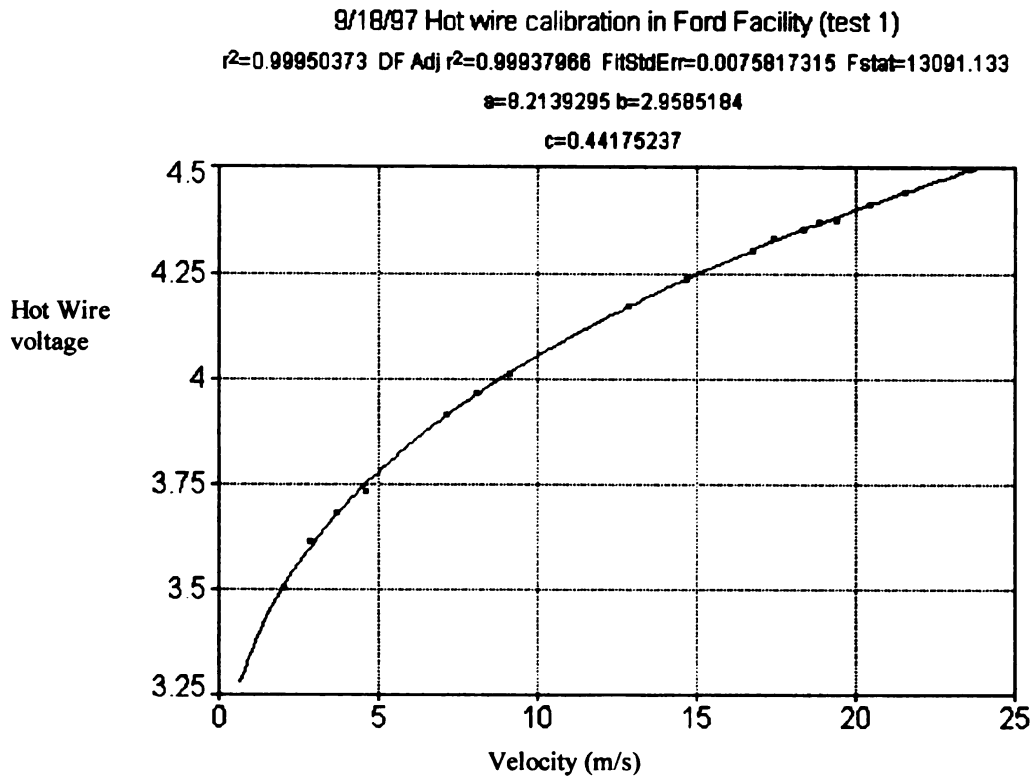


Figure 44. HTRL facility hot-wire calibration curve.

Hot-wire calibrations drift with time due to several factors such as oxidation or stretching or damage of the tungsten filament due to impacts with particles. It is absolutely necessary to calibrate the hot-wire prior to its use. Post calibration is desirable as well if the hot-wire survived the experiment. The two calibration data sets define a drift that the hot-wire experienced over time. It is necessary to perform this calibration every time a hot-wire is used and after approximately 3 hours of operation (due to oxidation) in order to insure that accurate measurements can be taken. The data set from the first calibration is used to define the operating parameters and the post calibration data is strictly used to define the amount of deviation that has occurred relative to the operating

parameters used for the experiment. These two calibration data sets define the maximum accuracy of the velocity measurement possible with the hot-wire for that experiment.

For example, Figure 44 shows the calibration curve for a hot-wire used in an experiment. The same hot-wire was re-calibrated after two and a half hours with the resultant data shown in Table 10. These hot-wire voltage data and pressure (velocity) measurements from the post-calibration are then used with the curve-fit data from the pre-calibration to define an error or drift quantity.

Table 10. Post calibration data

Velocity (m/s, via Equation 23)	Hot-wire Postcalibration Output (V)	Velocity predicted by Precalibration curve (m/s)	% Error
1.89	3.5	2.01	6.4
3.09	3.63	3.22	4.1
4.09	3.7	4.03	1.4
4.76	3.76	4.81	1.1
6.04	3.85	6.16	2.0
9.56	4.026	9.49	0.7
11.38	4.11	11.42	0.4
13.85	4.19	13.5	2.6
14.44	4.218	14.29	1.1
16.63	4.28	16.13	3.1
17.37	4.313	17.17	1.1
18.17	4.345	18.22	0.3
19.26	4.371	19.11	0.8
19.81	4.39	19.78	0.2
21.07	4.4	20.13	4.6
21.82	4.44	21.61	0.9

The mean of the error is 2.7%. Therefore, a measured velocity of 10 m/s for this test can be reported as $10 \text{ m/s} \pm 54 \text{ cm/s}$ with a 95% confidence level. This error term does not incorporate variance that occurs during the experiment itself (due to a surging compressor) so discretion must be applied by the experimenter to insure accurate reporting of uncertainty.

APPENDIX 5. MAXIMIZING THE DYNAMIC RESPONSE OF THE INFRAMETRICS IR CAMERA AND DATA RECORDING SYSTEM

Previous experiments by members of the Heat Transfer Laboratory have shown that the equipment used to record data from the Inframetrics IR camera effects the data. Following is a brief summary and recommendation from experiments run to optimize the dynamic range of the system.

It was found that the Panasonic AG-2400 VCR effected the data stream from the IR camera. It would seem obvious that the conclusion should be to replace this piece of equipment. However, the Panasonic AG-2400 VCR *increased* the dynamic range. The For-A VTG-33 video timer and the Sony PVM-1343MD Trinitron monitor did not effect the data stream. The raw signal from the Inframetrics camera has too much offset which results in an upward shift of the gray scale as a function of temperature output. This results in a reduction of the dynamic range capabilities of the system. Tests show that as much as 40% of the dynamic range was being loss by the previous equipment configurations being utilized.

The recommended equipment configuration for data recording and playback are as follows:

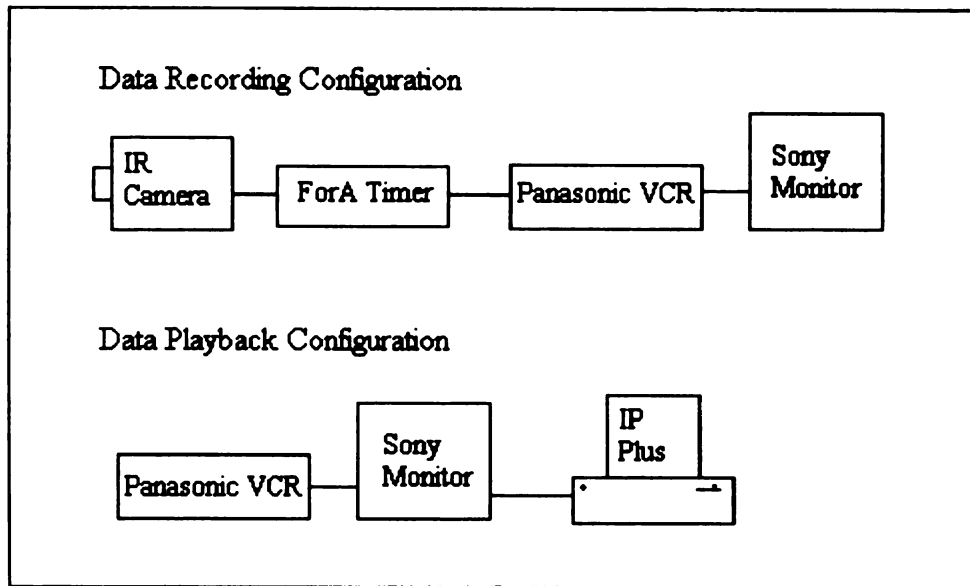


Figure 45. Optimal equipment configurations for data acquisition and processing.

On IP Plus Software:

Set Brightness to 48

Set Contrast in the range of 66 to 70

Set Gamma Function to 1.0 (this is the default setting)

On For-A Video Timer:

Set 75 Ω switch to ON

This arrangement resulted in obtaining 96.8% of the systems available dynamic response to temperature input. The results obtained and a comparison to the ideal system response are shown in Figure 46..

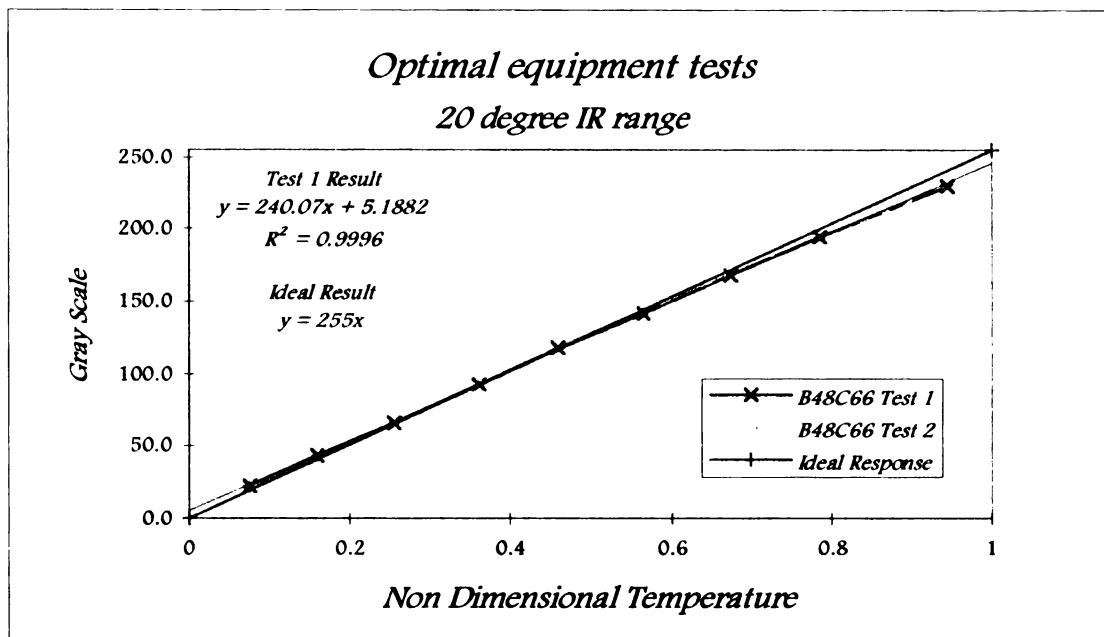


Figure 46. Results of optimized equipment configuration on gray scale - temperature relationship.

APPENDIX 6. VELOCITY AND TEMPERATURE CALCULATION PROGRAM FOR TWO HOT-WIRE METHOD

The following is a program written in Mathematica[®] to calculate the velocity and temperature from the data obtained from two hot-wires positioned in the flow field. The program solves for velocity and temperature values in an iterative fashion.

```
Clear[a1,a2,b1,b2,ts1,ts2,tinf,v1,v2,v,E1,E2,n1,n2,alpha,Rc1,Rc2,Rh1,Rh2,delta]
```

```
(** Iterative Solution for hot wire measurements of velocity and temperature**)
```

```
(** Input Room Temperature at Calibration **)
```

```
tcal1=22.9;
```

```
tcal2=23.0;
```

```
(** Input Parameters for specific wires and specific data points **)
```

```
E1=3.454;
```

```
E2=2.869;
```

```
A1=7.1596309;
```

```
B1=2.9114248;
```

```
n1=0.4197877;
```

```
Rc1=2.32;
```

```
Rh1=3.94;
```

```
A2=5.1325372;
```

```
B2=1.4904883;
```

```
n2=0.45644473;
```



```

Rc2=1.99;

Rh2=2.59;

ts1=(Rh1/Rc1)*(273+tcal1);

ts2=(Rh2/Rc2)*(273+tcal2);

delta=.005;

a1=A1/(ts1-tcal1);

b1=B1/(ts1-tcal1);

a2=A2/(ts2-tcal2);

b2=B2/(ts2-tcal2);

vel1[tinf_]=(((E1^2)/(ts1-tinf)-a1)/b1)^(1/n1);

vel2[tinf_]=(((E2^2)/(ts2-tinf)-a2)/b2)^(1/n2);

Plot[{vel1[tinf],vel2[tinf]},{tinf,15,35}]

tinf=15;

Do[{v1=(((E1^2)/(ts1-tinf)-a1)/b1)^(1/n1),

    v2=(((E2^2)/(ts2-tinf)-a2)/b2)^(1/n2),

    v=Abs[v2-v1],

    If[v<delta,i=5000,tinf=tinf+.0075]}},{i,4000}]

"Temperature (C)"

N[tinf,5]

"Velocity (m/s)"

"=Hot Wire1 velocity" v1

"=Hot Wire2 velocity" v2

```

"=Hot Wire velocity, average" $N[(v1+v2)/2,5]$

(** Output **)

2.35719 =Hot Wire1 velocity

2.35308 =Hot Wire2 velocity

2.3551 =Hot Wire velocity, average

BIBLIOGRAPHY

AISN Software Inc., TableCurve 2D v.3.05 for Win32, San Rafael, CA, 1994

Blevins, Robert D., Applied Fluid Dynamics Handbook, Van Nostrand Reinhold Company Inc., New York NY, 1984 p. 136-138, 312-316

Daryabeigi, Kamran, Wright, R.E., Puram, C.K. and D.W. Alderfer, "Directional emittance corrections for thermal infrared imaging", *Thermosense XVI*, SPIE Vol. 1682, 1992 p.325-331

Foss, J, M. Potter, Fluid Mechanics, Great Lakes Press, Inc. Okemos MI, 1982, pp.49-50

Gartenberg, Ehud and A. Sidney Roberts Jr., "Influence of Temperature Gradients on the measurement accuracy of IR imaging systems", *SPIE Vol. 1313, Thermosense XII*, 1990, p.218-224

Herring, Robert J., "Achieving high temperature measurement accuracy over a wide ambient temperature range in thermal imaging radiometers", *SPIE proceedings from Infrared Imaging Systems: Design, Analysis, Modeling, and Testing III*, SPIE Proceedings Vol. 1689, WA 1992

Holst, Gerald C., Testing and Evaluation of Infrared Systems, JCD Publishing Co., Maitland FL, 1993

Inagaki, Terumi, Suzuki, K. and Y. Okamoto, "Uncertainty Analysis of Surface Temperature Measurement Using Infrared Radiometer", *Thermosense XVI*, SPIE Vol. 2245, 1994 p.262-273

Incorpera, F. and D. Dewitt, Fundamentals of Heat and Mass Transfer, John Wiley and Sons, NY, NY, 1990, pp. 408-417, 708-749

- Inframetrics Inc., Model 600 Operator's Manual Document #05250-200 Rev C, Inframetrics Inc., N. Billenica, MA, 1988
- Inframetrics Inc., How Many Spots Make a Picture?, Inframetrics reports, Inframetrics Inc., N. Billenica, MA 1994
- Lafferty, John F., Arnold S. Collier, Infrared Surface Temperature Measurement in NAVSWC's HyperVelocity Wind Tunnel #9, ICIASF Record, IEEE, NJ, 1991, pp. 167-177
- Mandel, John, The Statistical Analysis of Experimental Data, Dover Publications Inc., NY, 1964 p.23
- Media Cybernetics L.P., *Image-Pro Plus* ® version 1.3 for windows, Silver Springs, MD, 1995
- Microsoft Inc., QuickBasic Version 4.50, Seattle Washington, 1988
- Miller, Irwin and Freund, J., Probability and Statistics for Engineers, Prentice-Hall, NJ, 1965, p. 166
- Morel, Thomas, "Design of Two-Dimensional Wind Tunnel Contractions", *Journal of Fluids Engineering*, Vol. 99, June 1977
- Okamoto, Yosizo and Terumi Inagaki, "Thermal Measurement Techniques of IC package Boards by means of Infrared Radiometer", SPIE Vol. 2245 Thermosense XVI, 1994, p.231-240
- Russ, John C., The Image Processing HandBook Second Edition, CRC Press, Ann Arbor MI, 1995
- Valvano, J.W. and Pearce, J. "Temperature Measurements", Optical-Thermal Response of Laser Irradiated Tissue edited by Welch, A.J., and van Gemert, M.J.C, Plenum Press, NY, NY, 1995, pp. 520 - 529.

White, M.J., The Development of Non-Contacting and Non-Destructive Experimental Techniques Capable of Measuring the Thermal Diffusivity of CVD Diamond Film, A thesis submitted to Michigan State University, 1996, pp. B1-B4

White, Matt, *Measurement of Slit Response Function*, Internal Laboratory Document - A30 RCE, Michigan State University, 1996

Willenborg, Klaus, Investigation of the Velocity and Temperature Fields of a Model Defroster Flow, Studientarbeit, Rhienisch-Westfälische Technische Hochschule, Aachen, Germany, 1996

Weast, Robert C., CRC Handbook of Chemistry and Physics 66th Edition, CRC Press, FL, 1986, p. F-89

Welch, A.J., and van Gemert, M.J.C., Optical-Thermal Response of Laser Irradiated Tissue, Plenum Press, NY, NY, 1995, pp. 520 - 529.